d Collection

공학석사학위논문

Imaging Payload System Design for Nano-Satellite Applications in Low-Earth Orbit

지구 저궤도 나노위성을 위한

영상탑재체 시스템 설계

2016년 8월

서울대학교 대학원

기계항공공학부

압하스

Abstract

This study presents a complete hardware and software design of an imaging payload, InterFace Camera (IFCAM), for the CubeSat standard. The payload is intended to take earth images from 350km Low Earth Orbit and is a non-critical mission payload for Seoul National University's first CubeSat, SNUSAT-1. The camera has a MT9D111 2M pixel image sensor with a STM32F429ZI processor running at 180MHz, 4GB SD card for data storage, 8MB flash memory and 8MB expandable SDRAM.

The camera is configured to take images in 160x120 pixels because of the limited downlink budget given to the imaging payload. Edmund Optic's fixed focus M12x0.5 lens with 650mm IR-Cut off filter and the Ground Sampling Distance (GSD) is calculated to about 650km. The Ground Swath, with the optics, is 570x400km which cover South Korea. The payload underwent Random Vibration and Vacuum Testing and showed no issues in the design. Furthermore, the design proposed is modular and has been used for designing the On-Board Computer for SNUSAT-1.

Keywords: CubeSat, Imaging Payload, Remote Sensing, Modular Design
Student Number: 2014-25145

Table of Contents

List of Tables

List of Figures

1. Introduction

Seoul National University's first satellite, SNUSAT-1, is categorized as a nano-satellite and is based on the CubeSat standard. The standard was first envisaged by Prof. Jordi Puig Suari at Cal Poly-San Luis Obispo and Prof. Bob Twiggs at Stanford University. The standard specifies that a 1-unit (1U) CubeSat shall have a volume 10X10X10 cm^3 and shall not weigh more than a 1.33kg. The SNUSAT-1 is a 2U CubeSat.

One of the secondary missions of SNUSAT-1 is to take earth images from 350km in Low Earth Orbit (LEO). For that, an imaging payload has to be in the satellite. SNUSAT-1's imaging payload InterFace Camera (IFCAM) is not mission critical, however, has important significance in in-house technology development. A qualified space camera can be used for star tracking for attitude control, debris monitoring, space rendezvous checking and remote sensing. For a practical example, the experience gained through developing IFCAM has been used for SNUSAT-2's primary payload Autonomous Space Vision System (ASVINS) for remote sensing and for the star tracker development, Arcsecond Pico Star Tracker (APST).

1.1. Previous Work

The focus has been on using Commercial Off-The-Shelf (COTS) components. For the author's undergraduate thesis, a feasibility study of GoPro Hero 4 sports camera for space environment was conducted. The camera was stripped down and a custom structure was built around the core electronics. Although thermal and stress analysis were done on SolidWorks, no real environmental tests were conducted on the camera [Maskey, 2014]. Furthermore, the camera was not selected as SNUSAT-1's IFCAM and instead decision was made to build a camera from scratch.

More influential work came from EstCube, Estonia's first CubeSat for initial hardware design. The camera was based on a STM32F2 ARM Cortex M3 processor with a custom built aluminum module weighing 30g. The camera had a 4.4mm telecentric lens with a 10 bit Video Graphics Array (VGA) resolution image sensor [Kuuste et al., 2014]. A detailed documentation of the work was later published by H. Kuuste in his undergraduate thesis. The camera functioned properly in space and image was obtained.

K. Gulzar had also designed a general propose imaging payload for pico and nano satellites on his Master's thesis [Gulzar, 2009]. The camera he designed was based on LPC2468 processor and used OV7720 image sensor. At the point of writing his thesis K. Gulzar was able to obtain images, verify outdoor test conditions but did not do any space environment testing.

A project group under the name 06gr415 from Institute of Electronic Systems of Aalborg University have published a detailed, theory intensive report on Camera System for Pico Satellites. The camera design study was made for AAUSAT-III satellite and is based on FPGA and ARM processor core. The report, however, concluded that no clear image was obtained during the study [Dalsagar et al., 2006].

Japan's involvement in CubeSat from the very beginning has produced a host of space qualified cameras. Japanese satellites XI-IV and XI-V each had a camera based on a PIC16 processor running at 10MHz. The CMOS based camera's image resolution was 0.3MP. XI-IV and XI-V were successful in taking images and transmitting them to earth [Kuuste, 2012, p.8]. Nano satellites from Tokyo Institute of Technology's CUTE-1.7+ APD II and Tokyo University's PRISM were also able to capture images [Kuuste, 2012, p.8].

Prof. Shinichi Kimura from Tokyo University of Science has been specializing in miniature space cameras as shown in Fig. 1. His cameras have gone abroad, International Space Station (ISS) [Watanabe, 2014, p.38], IKAROS [Kimura, 2013] solar sail mission and have now been successfully implemented on micro satellites Hodoyoshi 3/4 as a remote sensing payload [Terakura & Kimura, 2013]. His cameras have been based on PIC microcontrollers and FPGA and have incorporated both COTS sensors from On Semiconductor's MT9T line [Terakura et al., 2013] and Omnivision [Kimura, 2011, p. 20].

Figure 1 Modular miniature cameras from Kimura Laboratory, Tokyo University of Science

1.2. Requirement

Any design has to be constricted by requirements. In other words, system has to be requirement driven in power, mass and volume for optimized design. IFCAM has been designed according to the following requirements:

SS1-IFCAM-001: The mass has to be <100g
SS1-IFCAM-002: The volume has to be under 60x50x50 mm
SS1-IFCAM-003: The power consumption has to be <500mW
SS1-IFCAM-004: The Ground Swath shall at least be able to cover South Korea
SS1-IFCAM-005: The design has to be flexible and re-useable

1.3. Imaging Payload Structure

An imaging payload structure consists of optics, image sensor and processing board. The optics is responsible to converge parallel light onto the sensor. The sensor then converts the incident light to digital signal. The processing board reads that digital signal, processes the image and stores it on non-volatile storage. This section breaks down on optics and image sensors and highlights the basics.

1.3.1. Optics

Light entering the optics is considered parallel as subject on focus is placed at infinity. Parallel light beams enter the lens and bend due to refraction. Refraction occurs when the speed of light changes when entering one medium to the other. Convex lens bend light inwards [Serway & Jewett, 2004, p.36]. The imaginary point where these bent light intersect is called focal point. The distance between the focal point and the center of the lens is the focal length.

Aperture is an opening of the lens that limits incident light. The ratio of focal length f and diameter of the aperture D is the f-number of the lens. The f-number is symbolized as f# or simply F. Given that the f remains constant, lower f# indicates larger D which in turn allows more incident light to enter.

1.3.2. Image Sensors

Charge Couple Device (CCD) and Complementary Metal Oxide Semiconductor (CMOS) are two types of image sensors in digital cameras. While both types of sensors convert light into electric charge and process into electronic signals, in CCD

every pixel charge output is collected on a buffer and then transferred out from the chip as an analog signal. This requires a separate component for Analog to Digital Conversion (ADC), clock and timing generation and bias voltages. On the other hand, due CMOS's fabrication technique, all of the above components can be integrated onto the chip. This reduces power consumption and space.

Comparison shown in [Dalsagar et al., 2006, p.30] shows CCD to have highest Signal to Noise ratio, highest quantum efficiency, flexible integration and small pixel size while CMOS has one bias voltage, smallest sensitivity to radiation, easy integration of circuitry and low power consumption.

1.4. Remote Sensing

According to SS1-IFCAM-004, IFCAM is taking earth images which, in proper term, is called remote sensing. When information of an object, case in point being earth, is collected without making any physical contact of that object is called remote sensing. In case of IFCAM, the image sensor is the device that collects information through light reflected through earth's surface (or clouds). The camera is a single sensor device with a bayer filter enabling to sample images in Red (R), Green (G) and Blue (B) portion of the visible portion of the electromagnetic spectrum. The image sensor could also be sensitive to Near Infra-Red (NIR) in which case an IR cut filter is required. Since, data from two or more spectrum is collected, the type of remote sensing that IFCAM is undertaking is called a Multi-Spectral (MS) remote sensing.

There are two further terminologies that are important to understand for IFCAM. The Ground Sample Distance (GSD) is the physical representation of one pixel of the image sensor on the ground. GSD depends on pixel size, focal length and the altitude of the satellite. GSD is related to image resolution; lower the GSD, higher the resolution of the image. Ground Swath (GS) is the physical representation of the whole sensor on the ground. GS depends on sensor size, focal length and the attitude of the satellite.

GSD and GS can be calculated through the same procedure. For GSD,

$$\text{GSD} = \frac{a \times h}{f} \qquad (1)$$

where,
a = pixel size
h = altitude of the satellite
f = focal length of the lens
GSD value is given in *m.*

4

For GS, two similar calculations need to be done for a rectangular sensor. One in the x-axis and another in the y-axis. An example of how the GS can be calculated is shown in the Fig. 2

$$GS = \frac{a \times h}{f} \qquad (2)$$

where,

a = sensor size in x-axis or y-axis

h = altitude of the satellite

f = focal length of the lens

GSD value is given in *km*.
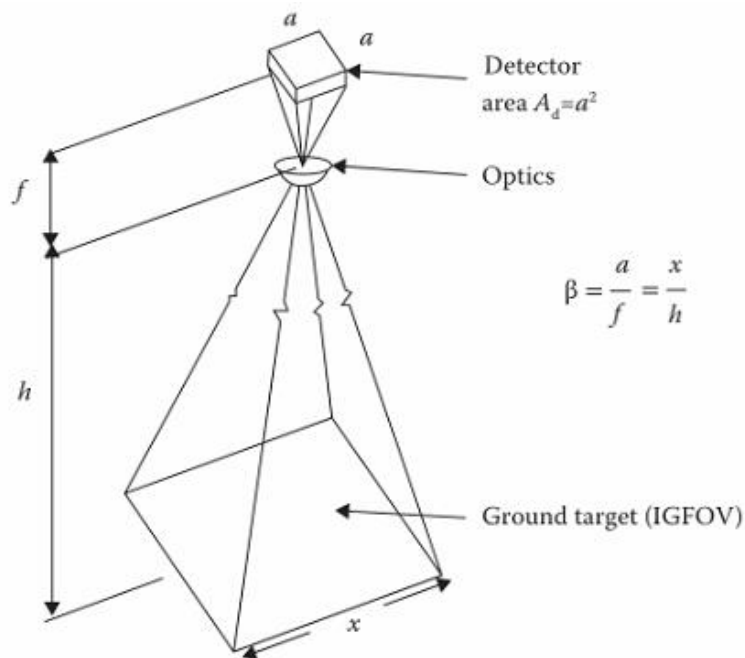
Figure 2 How GS (Instantaneous Geometric Field of View, IGFOV) can be visualized for calculation for a square detector of length *a*. **β** is the ratio of length by height which remains constant (Joseph, 2005, p32).

1.5. Space Environment

Space environment is considered extreme to the environment inside the atmosphere. Components which are manufactured for use on earth are susceptible to radiation and thermal extremes in vacuum condition that space imposes. Furthermore, space environment also includes the launching phase where the satellite has to

withstand a 6-axis vibration, and the shock that is created during the separation phases. Engineers and designers have to consider all these factors into their equation while designing and testing their system on simulated environments for risk management. A description of each of the conditions in space that could potentially lead to mission failure are included in this section.

1.5.1. Radiation

Charged particles are of various types and generated through different sources such as trapped particles in Van Allen Belt (VAB), and transient sources such as Solar Particle Events and Galactic Cosmic Radiation (GCR) [Muruganandan, 2014, p.9]. Particles include protons, electrons, heavy ions and alpha. SNUSAT-1's orbit is categorized as a sun synchronous orbit at 350km Low Earth Orbit (LEO) and has to take radiation from VAB and GCR into close consideration.

LEO satellites at 350km orbit are within the safety of the magnetic field, however, the satellite is bound to pass over the South Atlantic Anomaly (SAA) [Botma, 2011]. Particles from the inner VAB contributes primarily to SAA. The effect could affect orbits as low as 250km above the Atlantic Ocean off the Brazilian Coast [Coderre, 2016, p.8].

Devices exposed to radiation degrade, exhibit background noise in detectors, induce electrostatic charge and create errors in digital circuits. These effects can be categorized into Single Event Effects (SEE) such as Single Event Upsets (SEU) and Single Event Latchup (SEL), and Total Ionizing Dose (TID). SEU occurs when a charged particle causes a change in content and/or state of a device without causing permanent damage to that device [Grobler, 2000]. SEL occurs when radiation causes a parasitic transistor within the device to switch on which results into excessive current flow [Grobler, 2000]. The collection of radio-active particle on the device over time due to exposure to constant radiation is known as TID. The tolerance is seen as a measure to determine the life expectancy of an electronic device [Grobler, 2000].

1.2.2. Thermal Vacuum

SNUSAT-1 will be deployed at 350km LEO. The thermal vacuum environment is described as earth rarefied atmosphere with extremely low density and pressure (3-5 10^{-6} Pa). At this altitude, the gravity trapped gas layer absorbs heat from Ultra Violet (UV) of solar radiation [Martinez, 2016]. The main mode of heat transfer to the satellite is radiation while both conduction and radiation play a part in heat transfer inside the satellite. Source of heat through radiation are direct sunlight,

albedo and thermal energy radiated from earth.

Sunlight is primary source of heating of satellites. The intensity of sunlight at Earth's mean distance from the sun (1AU) is known as the solar constant and is equal to 1367W/m^2. This value is recommended by the World Radiation Center in Davos, Switzerland, and is believed to be accurate to within 0.4% [Gilmore, 2002, p.22]. A sunlit surface can expect a temperature of 110°C~130°C all year round in LEO.

Albedo is the sunlight reflected from earth's surface. Albedo is quantified as a fraction of incident sunlight reflected back to earth. Depending on variation of latitude, the Earth's Albedo α can lie anywhere between 0.31~0.39. Thermal energy from earth is reflected through Infra-Red (IR). Low Earth IR values tend to be associated with high albedo while high Earth IR tends to be associated with low-to-moderate albedo [Gilmore, 2002, p.30]. Therefore, during hot case calculation, a simplified approach is to ignore heating from Earth IR and only consider worst case albedo.

One region where Earth's IR has to be considered is when the satellite enters an eclipse. At this point, the only source of heat is Earth IR. Taking into the consideration that the satellite is exposed to 175W/m^2 from radiation from earth, a satellite can be exposed to up to -170°C in LEO [Gilmore, 2002].

The extreme variation in temperature in space poses critical design challenges for an engineer designing the system. Thermal fatigue due to thermal stress or brittleness due to cold could compromise the structural integrity of the satellite. Besides this, the thermal vacuum condition could lead to outgassing. Outgassing is the process of particles in a medium ejecting out due to conditions in space. These particles could then deposit on sensitive instruments such as solar arrays or imaging sensors which could cause mission failure. Furthermore, formation of tin whiskers in vacuum has also been a cause for concern for short-circuit related accidents.

1.2.3. Vibration

Before SNUSAT-1 reaches LEO, the satellite has to be launched to space. Space launch vehicles such as the Space X's Dragon or Ariane Space's Ariane 5 take payloads to LEO and Geostationary Orbit (GEO). Launch conditions in beginning of the launch to stage separation pose their own unique dynamic environment that payloads strapped inside the rocket need to tolerate. This can be severe for structure and components and could result into fatigue and damage.

The source of the vibration can be characterized as mechanical, acoustic and aerodynamic. Mechanical vibrations come from equipment, thrust change and separation of stages. Acoustic vibrations channel from engine and are maximum within few seconds of liftoff [Aggarwal, 2011, p.3]. Aerodynamic vibrations source

from pressure fluctuations in the turbulent boundary layer, flutter of a fin or panel in the airstream due to dynamic instability among other causes [Aggarwal, 2011, p.3].

Engineering Qualification Model (EQM) and Acceptance Test Model (ATM) undergo random vibration, sine vibration, sine burst, shock and acoustic tests on given specification by launcher. ATM undergoes Maximum Predicted Environment (MPE) while EQM undergoes testing up to 6σ. While these testing are only done an axis at a time, the data present engineers a good understanding of satellite's structural and hardware integrity.

2. Hardware

2.1 Design Constraint

2.1.1. Requirements

The imaging payload in SNUSAT-1 is not a mission critical payload. The secondary mission states that the camera has to take earth images and accordingly, the processing hardware, sensor and optics should be selected and designed. SS1_IFCAM_004 states that the GS has to cover South Korea (approx. 400 X 300 km) while no restriction on GSD is imposed.

SS1_IFCAM_001/002/003 specifically state the mass, volume and power requirements respectively for the imaging payload. An analysis as to whether or not the camera has fulfilled the requirement will be discussed later in the Conclusion chapter of this thesis.

2.1.2. Downlink Budget

One major bottleneck for image size is the downlink budget. The downlink speed is given to 5000bps. Given that a single pass is estimated to communicate for 10 minutes and 10% of that time is allocated for image data, the total amount of data that can be download in a single pass is 37KB. To put the situation under perspective, a single RGB565 image in QQVGA format has 38.4KB data. If onboard image processing is implemented, a minimum of two passes are required to download a full image. Both hardware and software should take this into consideration. How this has affected the hardware design will be discussed in the upcoming sub-chapters.

2.1.3. Availability

While prototyping, one major hurdle is to find components that are readily available in the market that fit the requirements imposed. If not, delays are inevitable. Therefore, a tradeoff should be placed while selecting components that are readily available in the market. Additionally, availability of development boards and

modules should also be considered in order to reduce development time and facilitate ease of software development.

2.1.4. Reliability over Cost

In space, due to the harsh environment, the camera is exposed to radiation and wide range of temperature. Furthermore, the camera's structural integrity should remain intact while launching and separation. While cost can be an issue for small, pico-scaled satellite projects like SNUSAT-1, investment should be made in proper hardware to ensure the camera does not lose its integrity. Consideration on reliability has been discussed in the subsequent sub-chapters.

2.1.5. Modularity

Hardware design should consider modularity for other sub-systems and future missions. This reduces development time, facilitates sharing of code and places less burden on designers. An explanation on how the design has been reused is provided in the Conclusion of this thesis.

2.2. Hardware Selection

2.2.1. Processor

A. Camera Performance Criteria

A camera processor's performance is based on two factors:
1) Volatile memory (RAM)
2) Performance of MCU
The previous chapter touched on the selection and design process of image sensor and its module. The remaining two factors are based on the MCU. While an external RAM can be interfaced with the MCU, a processor with higher internal RAM with higher performance is desirable. Unfortunately, an important tradeoff between selecting higher performance MCUs is that they consume more power. A proper market study has to be done to explore if there are power efficient, performance based MCUs.

B. Market Study

There are wide range of MCUs in the current market. While 32 bit processors are slowly taking a significant chunk of the market share, 8-bit and 16-bit processors are still widely popular for cheap, low power applications. One important factor for 32-bit processors is that they can incorporate higher RAM. 8-bit are limited by RAM space and 16-bit processors can only address up to 64KB RAM. 32-bit processors can address up to 4GB RAM. 32-bit processors also have the advantage of having bigger program memory (1/2MB).

ARM Cortex M architecture has been widely implemented on MCUs by leading industries such as Atmel, TI, NXP and STM for their 32-bit processors. The architecture is known to be power efficient while delivering high performance. This is ideal for CubeSat missions where power is limited but require better processors. Besides this, an importance has to be given to processors which have a dedicated camera interface. While interfacing a camera without an interface is still possible through General Purpose Input Outputs(GPIOs), having dedicated hardware will ease development of software. During market study, MCUs with camera interface were only selected as shown in Table 1. Furthermore, a MCU with external memory interface, dedicated clock output and wide range of serial interfaces was preferred.

Table 1 Market study for processors with camera interface

Processors → Parameters			
Company	STMicroelectronics	NXP	Texas Instruments
Component	STM32F429	LPC4300	CC3200 (WiFi SOC)
Core	ARM Cortex M4 with FPU	ARM Cortex M4/M0 Dual Core with FPU	ARM Cortex M4
Speed	180MHz	204MHz	80MHz
Power Consumption (max)	323.4mW @ 180MHz	270.6mW @ 204MHz	917.4mW @ 80MHz
Operating Temp	-40℃ to +85℃	-40℃ to +85℃	-40℃ to +85℃
DMIPS/MHz	1.25	0.9	Not given
Coremark	608	595.93	Not given
Flash Memory	2MB	1MB	-
SRAM	256+4KB	282KB	256KB
External Memory Interface	Flexible Memory Controller (FMC)	External Memory Controller (EMC)	32-Channel Direct Memory Access (uDMA)
Clock Output	Yes	Yes	Not mentioned
Camera Interface	Digital Camera Interface (8-12bit)	Serial GPIO (8-bit)	8-bit Camera Interface
Communication Interface	SPI, I2C, USART, USB, CAN	SPI, I2C, UART, USB, CAN	SPI, I2C, UART
DMA	16 with FIFO	Available	Available
Power Mode	Sleep, Stop, Standby	Sleep, Deep Sleep	Idle, Traffic, Low Power Deep Sleep
Watchdog	Available, Independent	Available, Windowed	Available
Package	LQFP, BGA, WLCSP	LQFP, BGA	QFN
Dev. Board	Available, Cheap	Available	Available, Cheap

C. MCU Selection

Unlike TI's CC3200, STM's STM32F429 and NXP's LPC4300 both run at high clock rates. To draw conclusion on MCU performance solely on processing speed is not recommended. For this, benchmark scores are used. Two such popular benchmark scores are Dhrystone MIPS and CoreMark. CoreMark is thought to be better than DMIPS as CoreMark is independent of C library's performance. However, looking at these benchmark scores, STM32F429 has scored higher than LPC4300 on both test scores.

Camera performance also corresponds to RAM storage available. Both MCUs have similar RAM storage and have external memory interface. They both have Direct Memory Access (DMA) for uninterrupted data transfers and have low power modes to save energy. When all peripherals are turned on, the nominal consumption in STM32F429 is shown to be higher. Power consumption for CC3200 is nearly 1W and will not be considered further for camera design.

Generally, an image sensor has a serial interface for commands and register settings, data lines, clock lines and power input. For serial interface, Inter Integrated Circuit (I2C) is the standard. Besides that, having a camera interface and clock output in the MCU plays an important role in minimizing software development and use of additional component.

STM32F429 and LPC4300 have both I2C interface, camera interface with clock output. However, the important factor here is that the former processor has a flexible 8-12bit Digital Camera Interface (DCMI) as compared to latter's limited 8-bit Serial GPIO(SGPIO). This means that, in future, if the same processor was used to interface a sensor with 12-bit camera output, STM32F429 will be the only processor through which the design can be reused.

Focusing attention on STM32F429, the processor has Serial Peripheral Interface (SPI) for non-volatile storage, has a Low-Profile Quad Flat Package (LQFP) package for easy prototyping and a cheap development board to build software for the camera. MT9D111 image sensor can run at maximum speed of 80MHz. STM32F429's GPIOs can run at maximum speed up to 90MHz, and so forth can handle camera data without problems. Therefore, STM32F429 has been chosen as the ideal processor for the camera.

2.2.2. Image Sensor
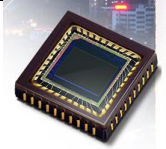
A. CCD vs CMOS

As discussed in the Chapter 1, there are two types of image sensors; CCD and CMOS. CCD image sensors has been the industry standard, however, the recent improvement in CMOS manufacturing technology has changed the landscape at the turn of the century. While CMOS sensors have higher Dynamic Range (DR), lower Uniformity and only better Responsivity than CCD sensors, they are more compact, have lower mass, consume less power and are potentially more radiation tolerant (Waltham, 2013, p.423).

B. CMOS sensors: Market Study

Two popular electronic component websites, www.eleparts.co.kr and www.devicemart.co.kr, were used for market research. Furthermore, domestic companies who produce image sensors were directly contacted. Image sensors from foreign companies Omnivision and On Semiconductor (formerly Aptina) and domestic companies such as Samsung, LG, PixelPlus and Clairpixel were studied. Due to small amount of image sensors that needed to be purchased for prototyping, Samsung and LG did not comply to sell their product, however, after much difficulty, image sensor POA030R from PixelPlus and USB module for CP8108 from Clairpixel were obtained. Ironically, purchasing image module of foreign companies was straightforward and was completed through the internet. Omnivision's OV2640 and On Semi's MT9D111 image modules were selected because their datasheets were available in the internet and no Non-Disclosure Agree (NDA) had to be signed. Table 2 shows all the image sensor available.

Table 2 Market study of available image sensors

Image Sensor → Parameters				
Company	On Semiconductor	Omni-Vision	ClairPixel	PixelPlus
Nationality	US	US	Korea	Korea
Sensor	MT9D111	OV2640	CP8108	POA030R
Optical Format	1/3.2	1/4	1/3	1/4
Full Resolution	1600 X 1200	1600 X 1200	720 X 480	640 X 480
Pixel Size	2.8um X 2.8um	2.2um X 2.2um	6.5um X 7.4um	3.6um X 3.6um
Shutter Type	Rolling Shutter	Progressive	Rolling Shutter	Progressive
Maximum Frame Rate	15fps	15fps	30fps	30fps
Max Clock	80MHz	Not stated	54MHz	27MHz
Output Format	YCbCr, RGB, JPEG (without headers), RAW 10 bit	YCbCr, RGB, JPEG RAW 8/10 bit	CCIR, YCbCr, RGB, RAW Bayer 10 bit	CCIR, YCbCr, RGB, RAW Bayer/Mono 9 bit
Responsivity	1.0V/lux-sec	0.6V/lux-sec	6.4V/lux-sec	2.93V/lux-sec
Dark Current	-	15mV/sec	-	25.2mV/sec
Dynamic Range	71dB	50dB	120dB	51dB
Signal to Noise Ratio (max)	42.3dB	40dB	43dB	44.2dB
Power Consumption	<348mW @ 15fps	<140mW @ 15fps	<311mW @ 60fps	<67mW @ 30fps
Operating Temp	-30℃ to +70℃	-30℃ to +70℃	-40℃ to +105℃	-30℃ to +80℃

C. Image Sensor Selection

Initially, for SNUSAT-1 imaging payload, POA030R and CP8081 image sensors were selected. This was done to give preference to domestically produced image sensors as opposed to using foreign COTS image sensors. However, documentation and support from domestic companies were poor with no user based community in the internet sharing problems and codes. This is important for university CubeSat projects as time and resource budget are highly constrained.

After unsuccessful attempts on PixelPlus' POA030R and ClairPixel's CP8081 (which have been documented in Chapter 2.4.3) OV2640 received attention. WaveShare produces image modules for the sensor and are widely popular. This is important for two reasons:

1) Having a working hardware aids in proper software development. Developing both simultaneously will create confusion as to where the problems lies, if any.
2) User base is large and have code available online.

After successfully receiving image data from OV2640, MT9D111 sensor from On Semiconductor was then selected because SNUSAT-2's selection of MT9P031 sensor from On Semiconductor. Importance was placed on gaining experience for future, more complex imaging payload mission. Although the power consumption for MT9D111 is higher than that of OV2640, the former has larger DR, higher Responsivity and can run at higher speed. MT9D111 also has an internal master clock generator and the camera speed can be reduced to lower power consumption. This is not possible with OV2640 sensor.

2.2.3. Optics

A. Market Study

Although optics is an integral part of any camera design, designing a custom optics is time consuming, labor intensive and a difficult procedure. Instead, COTS M12 X 0.5 lens were selected as the optics for the camera payload. Five different lenses purchased from www.devicemart.co.kr were analyzed to check what Ground Sampling Distance (GSD) and Ground Swath (GS) each lens would produce. The calculation assumed the orbital height as 350km, sensor size and pixel size of MT9D111, assumed the resolution to be in QQVGA format achieved through 4x skipping and 2x binning. The focus for all of the listed lens is fixed and is at infinity. Table 3 shows comparison between M12 X 0.5 mm lens.

Table 3 Comparison of M12 lens available at devicemart.co.kr.
For GSD and GS calculation, orbital height of 350, resolution of QQVGA,

Lens ———→ Parameter					
Component	2920PL001	3620PL001	6018PL001	8020PL001	1620PL001
Focal Length (mm)	2.9	3.6	6	8	16
Fixed focus	Infinity	Infinity	Infinity	Infinity	Infinity
AFOV (D)	120°	92°	60°	40°	16°
GSD (m)	675.86	544.44	326.67	245	122.5
GS (km)	545 X 412	439 X 332	263 X 199	197 X 149	98 X 74

B. Lens Selection

Since there is no specific requirement for GSD and GS, selection of optics was done so that an image can at least cover the South Korean peninsula. For this the GS has to be in around 400km X 300km. 3620PL001 fulfills this requirement and the test results for the lens have been provided in chapter Chapter 4.

2.2.4. Volatile Storage

Market study had shown that STM32F429ZI had an affordable development board available which is shown in Fig. 3. A development board is an electronic component which allows engineers to work on the hardware to evaluate the performance of the processor before building custom electronics. The development board for STM32F429ZI is the STM32F429I-DISCO board. The board houses a 144pin LQFP packaged STM32F429ZI, 2.4" QVGA TFT LCD and a 64Mbit IS42S16400J SDRAM from Integrated Silicon Solution, Inc. As the design is an open hardware and software design, example schematics with example application code is available. In order to simplify the design process, the same SDRAM was incorporated in the IFCAM design for volatile storage.
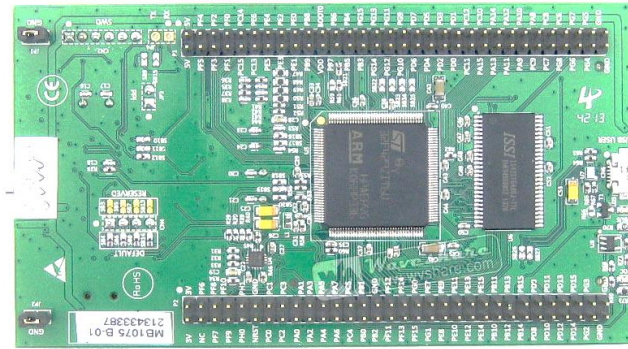
Figure 3 STM32F4-Discovery Board for easy prototyping

2.2.5. Non Volatile Storage

The camera design incorporates two non-volatile data storage for redundancy. 64Mbit SST25VF064C SPI serial flash from Microchip and Class 4, 4 GB micro-SD card from SanDisk as shown in Figure 4. Although STM32F429ZI has both SPI/SDIO for interfacing with micro-SD cards, SPI is selected as the same SPI can be used for micro-SD and flash.

Figure 4 Non-volatile storage on IFCAM

2.3. Hardware Design

2.3.1. Processor/Camera Connection

MT9D111 image sensor has five major hardware connections:
Data output: MT9D111 can output 10-bit data, however, only 8-bit RGB565 data is being utilized. D[0:7] has to be connected to the GPIO of the processor.
Clock Input: Also known as the master clock, the clock input is necessary for the camera to function. This input can be scaled to run the camera up to 80MHz.
Clock Outputs: HSYNC, VSYNC, LINE_VALID and PIXCLK are connected to the

GPIO of the processor.

Power input: MT9D111 module has a 3.3V input along with an input for GND.

Serial Command: MT9D111 uses I2C to set registers.

STM32F429ZI has these special peripherals which facilitate those hardware connections:

DCMI: The digital camera interface is connected to Data output line D[0:7] and clock outputs.

I2C: STM32F429ZI can act as the master and communicate with the MT9D111 through I2C.

MCO: Master Clock Output can provide stable clock signal to the camera's clock input.

Power for the MT9D111 is provided directly through a switched and regulated supply from Electronic Power System (EPS). The On-Board Computer can turn on or off the camera system using a switch.

2.3.2. Processor/SDRAM Connection

STM32F429ZI is connected to IS42S16400J through the processor's Flexible Memory Controller (FMC). The parallel interface allows seamless temporary data storage and access to the SDRAMs memory addresses.

2.3.3. Processor/Flash-uSD Connection

STM32F429ZI is connected to SST25VF064C serial flash through SPI. The processor acts as the master and can read and write data on the flash. The same SPI channel is also used to access the uSD card. Only one non-volatile storage can be accessed at a time.

2.4. Prototyping:

Prototyping is an integral part of designing a system. Once the hardware is understood, a hardware has to be built to demonstrate the proof of concept. The following methods should be considered to reduce time and wasteful effort while electronics prototyping.

Using development boards and modules: While developing, the engineer must have confidence either on the hardware or the software. Loss in confidence in both will create unnecessary confusion as to where the problem lies, if any. Using development boards or modules which are readily available in the market allows one to focus on software. After verifying the software works, one can approach designing

the hardware and "feed-backing" that software onto that hardware.

Refer to open hardware and software design: While copying is never encouraged, understanding how other people have approached designing an electronic system is key to building a better system. The internet has a lot of resource on open hardware and software, especially with STM32F microcontrollers and that played a crucial role while creating a blueprint for design.

Having PCB design skills: While BBM doesn't necessarily require to design a PCB, the final design must incorporate the PCB. For that, learning to design simple electronic circuits on PCB as earlier as possible is key. While a design can be outsourced, knowing how to build PCB will unconsciously reinforce concepts on packaging, current flow, capacitance, inductance and component placement.

Building soldering skills: Learning how to solder is one of the basic skills that an embedded engineer should have. This also means that he/she should be aware of what kind of flux to use, information on different soldering iron tips and what to use when, appropriate temperature for soldering and how to keep a PCB clean. For space application, one should be aware of what flux or soldering wire to use as whiskers could short the system.

2.4.1. PCB Design

A. Software

For SNUSAT-1 Camera design, PADS 9.3 was used to design the PCB as shown in Fig.5. The software comes in three bundles; PADS logic, PADS layout and PADS router. The process begins with building the library for components. A library consists of parts (component representation) and each part consists of information on decal (pcb footprint, package info) and logic (schematic diagram). While the software provides library for a range of electronic packages, using them directly without cross-checking is not recommended.
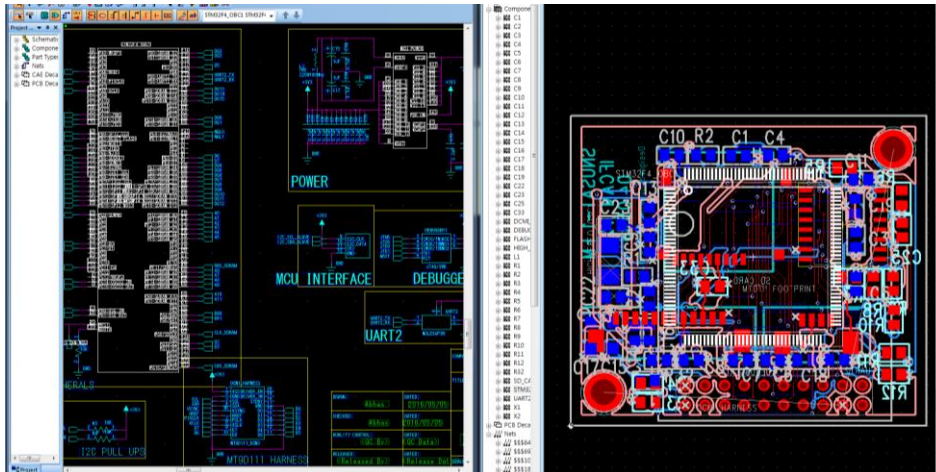
Figure 5 PADS 9.3 PCB design software (full picture refer Appendix)

After a library has been built of all the components needed for the camera, a logic schematics can be sketched on the PADS logic. This serves as the blueprint for the design. Once this is complete, the information is then exported to PADS layout. The software shows the physical footprint of the components and can be arranged according to the space available. The user can then select the trace width, define layers, create keepouts and place design rules for routing. Finally, the layout is then exported to PADS router where the digital connections between components are turned into traces. While auto-routing is not advisable, by carefully designing the layout and by setting appropriate rules, auto routing can achieve optimum results. A cross checking has to be done after each route.

B. PCB design rule-of-thumbs

Traces: power traces and high frequency traces should be as short as possible while avoiding using vias as much as possible. Additionally wider trace width for power traces is generally recommended.

Planes: power planes should be implemented if possible and if budget allows.

Spacing: Traces and components should be at least 50mil away from the board outline. Vias should be placed at about 15mil away from traces, pads and holes. Recommended distance between pads to pads, holes to pads, pads to trace and trace to holes is 10mil.

Trace width: For outer layer with 1oz copper pour, a trace width of 12mil is recommended for 1A of current flow in room temperature. For inner layers for the same amount of pour, 30mil has a current rating of 1A.

C. Good soldering practices

Grounding: Electrostatic discharge could potentially destroy sensitive components such as MCUs and image sensors. The person soldering should always remain grounded and should avoid placing his/her leg on the ground.

Soldering Temperature: Through experience, a temperature of up to 350℃ can be set for soldering iron.

Using Gloves: Avoids sweat and shorting components during soldering. Wearing latex gloves is recommended.

Cleaning: After soldering is complete can be done through isopropyl alcohol. However, if no clean flux is used, this not required.

Inspection: After completion, inspection of the pcb should be done to check for cold soldering and residues.

2.4.3. BBM Model

A. PixelPlus' POA030R Image Sensor

Initially, preference was given to image sensors from domestic companies. PixelPlus' POA030R did not have an image module and had to be built in-house as shown in Fig. 6. The company had provided schematics and datasheet. That design was implemented for prototype V1 and V2. The prototypes were connected to the DCMI port of STM32F429I-Disco board.
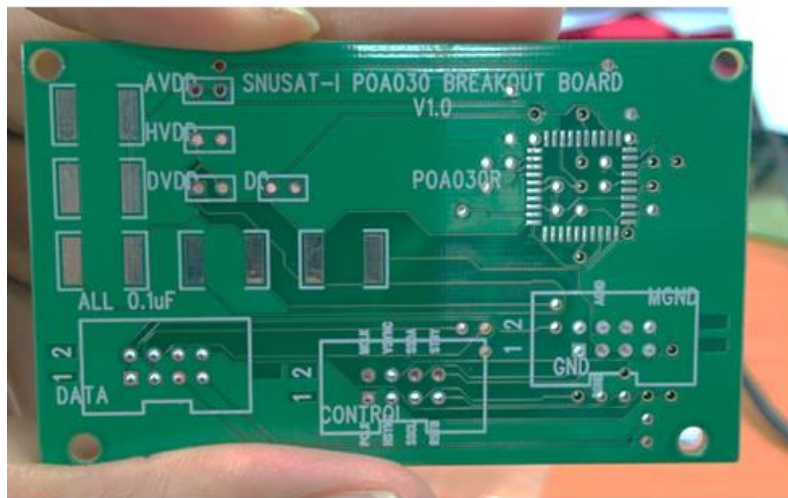
Figure 6 POA030R custom breakout board for BBM

V1.0 had certainly issues as 1) capacitors were placed further away from the sensor 2) the wires connecting the development board were long 3) the LDO regulators should have been placed on the same PCB. There were further unsuccessful attempts at I2C and the sensor was shown not to initialize. To improve that revision on the breakout board was made while also designing SNUSAT-1 Camera Development Board as shown in Fig. 7.
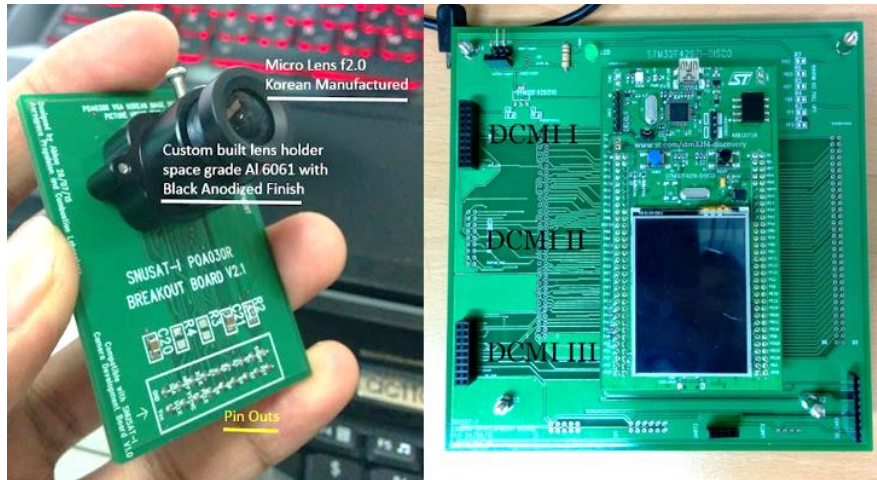
Figure 7 Improved Breakout board for POA030R (Left)
SNUSAT-1 camera development extension board for STM32F4-Discovery (Right)

In V2.x, the previous considerations on wire length, placement of capacitors and regulators were included and is shown in Fig.8. To reduce wire length between the camera and the development board, a STM32F29I-DISCO SNUSAT-1 Camera Development Board was built. The POA030R module could now be placed directly on the DCMI port (s) without additional wiring.
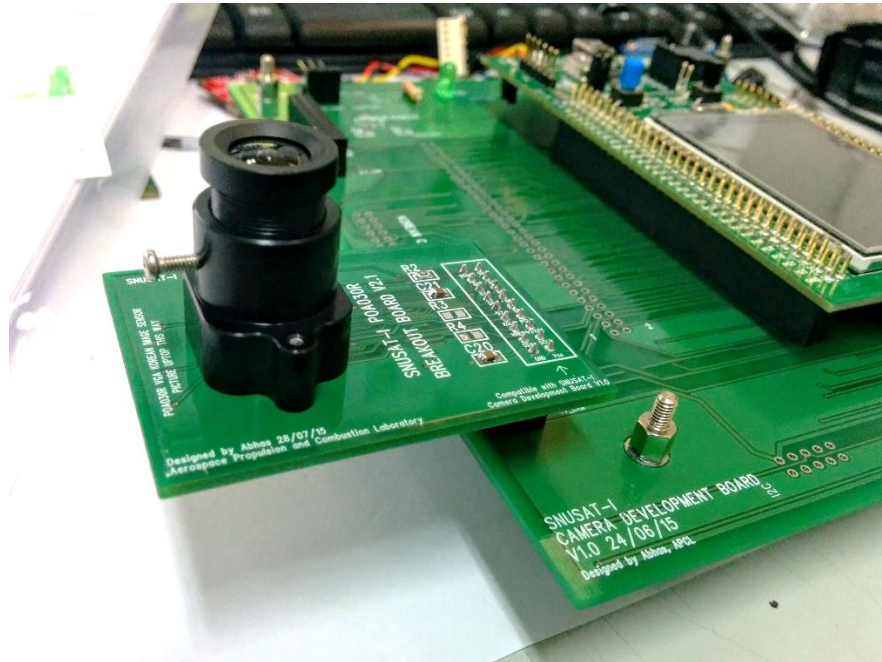
Figure 8 Minimizing wires and wire length for prototyping

For V2.x, the camera responded for I2C after giving an input clock of 8MHz. The register values were successfully written, however, no data was received. PixelPlus' support team provided further register values, however, the settings did not change the result. Furthermore, the datasheet was poorly documented. After several weeks of no results, the attention was then diverted to building a working BBM for camera processor instead.

B. STM32F429ZIT6 Camera Processor

Before building a PCB for the MCU, the design was implemented on a Bread-Board. The schematic design is based on open hardware designs that were available in the internet. The processor is the exact same MCU on the STM32F429I-Disco board. The LQFP 144 pin has both FMC and DCMI pins available. The reason for selecting such a large package is that the smaller package, LQFP 100, did not have the full FMC pins and additional component is required to multiplex the data and address lines. The simple solution would be to use a larger package with all the required peripherals. A simple test sketch was uploaded and checked to verify that the processor was responding.
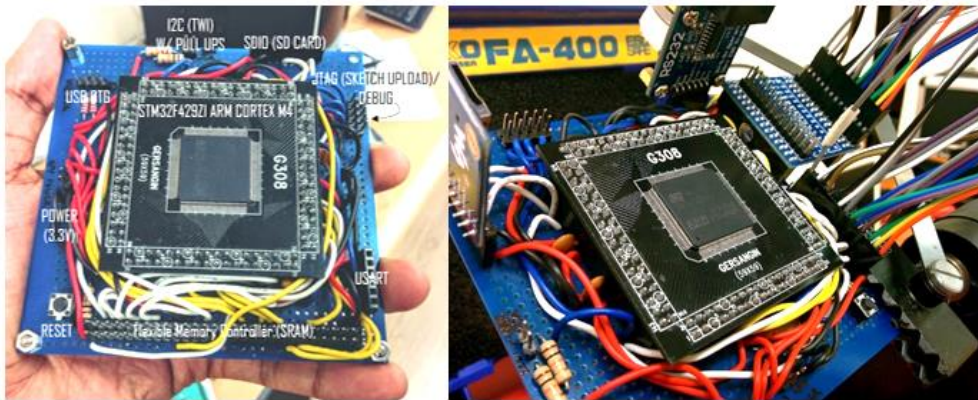
Figure 9 BBM of STM32F429ZIT6 processor

C. ClairPixel's CP8108

A USB module for ClairPixel's CP8108 was directly purchased from ClairPixel, another Korean which was willing to cooperate. The camera was interfaced with the BBM model of STM32F429ZI, however no enumeration was successful. The camera did respond in Windows 7 using commercial USB camera software but failed to work while interfacing with the MCU's USB OTG. Proper documentation and support was lacking and after unsuccessful attempts, the CP8108 module was abandoned. The module and the image obtained in windows is shown in Fig. 10.
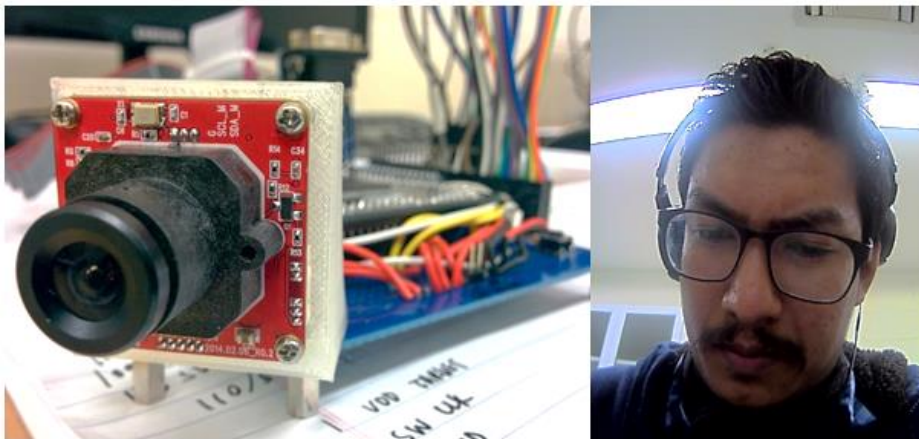
Figure 10 CP8108 USB module (Left)
and image obtained from the module in windows (Right)

D. OmniVision's OV2640

The OV2640 image sensor has a module, is well documented, has source codes available, and a larger share of embedded systems have utilized the sensor. The sensor has a similar initializing pattern through SCCB (I2C) and has an embedded JPEG encoder. Image from the module was successfully obtained after interfacing the camera with the STM32F429I-DISCO board plugged on the SNUSAT-1 Camera Development Board.
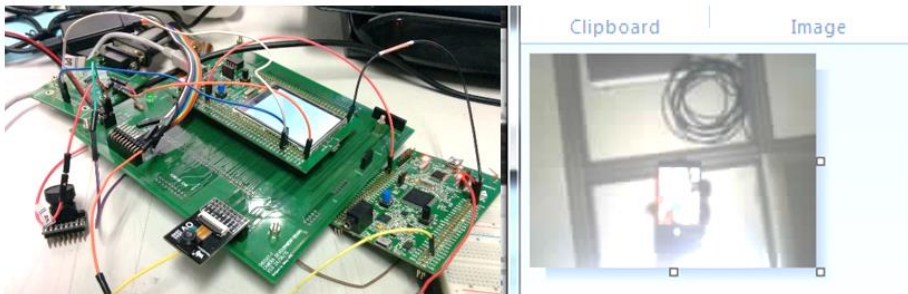
Figure 11 BBM model for OV2640 sensor (Left)
and JPEG image obtained from module (Right)

E. On Semiconductor's MT9D111

The MT9D111 image module is similarly popular in the embedded community. The datasheets are available without NDA and the online community have posted source codes on the internet. Furthermore, the On-Semi provides a registry generator for MT9D111 which simplifies software development significantly. Image data was obtained using the STM32F429I-DISCO board interfaced on the Open429Z-D expansion board from Waveshare.
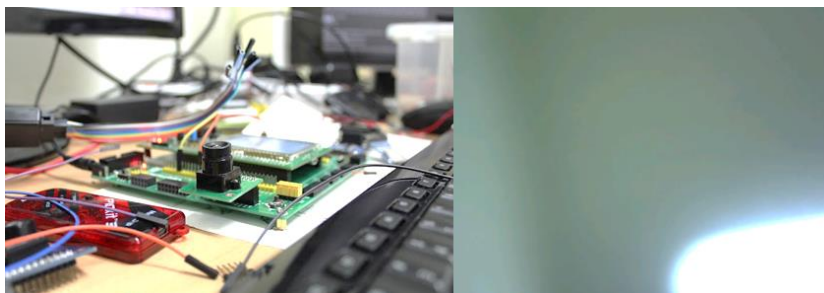
Figure 12 BBM model for MT9D111 sensor (L)
and first RAW RGB565 image obtained (R)

2.4.4. PCB Model

After testing the design on the BBM, the design can now be built on the PCB. The approach was to first build the camera processor PCB and then integrate the camera onto that model. ST-LINK/V2 in-circuit debugger/programmer was used to upload the sketch compiled by IAR Workbench. Results are shown in Fig. 13.
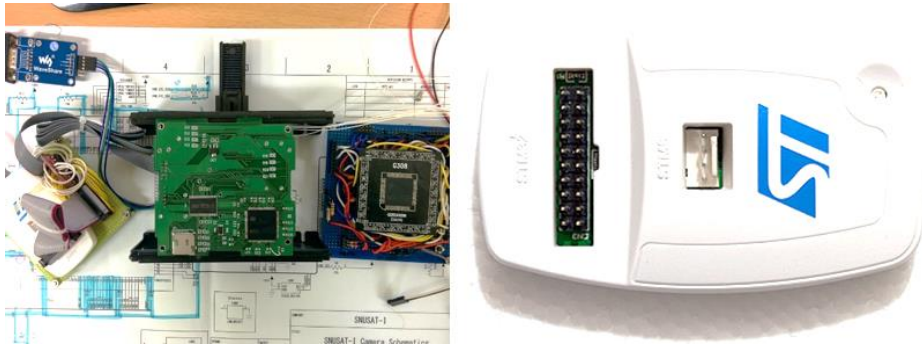
Figure 13 PCB implementation (Left)
with ST-LINK/V2 debugger/programmer (Right)

The camera electronics, excluding the image sensor, were integrated to SNUSAT-1's IF1(Interface Board 1). There were some issues 1) Camera was not modular. A modular imaging system would allow different sensors to be placed on IF1. 2) Took PCB space on the IF1. 3) The design was tightly coupled to other components on IF1. This increases the risk for failure. 4) No consideration for Electro-Magnetic Interference (EMI), ground shielding or proper capacitor placing done.

Taking these factors into consideration, a modular camera dual PCB (MT9D111 image module and camera processing board) was designed. The IFCAM V1.0 (Camera processor board) features a 4-layer PCB with two power planes for stable power, ground shielding for high speed external oscillator according to AN2867 document from STMicroelectronics. Placement of pull up resistors for SPI and I2C, inductor placement between analog and digital power inputs and capacitor placement was done in accordance to AN4488 also from STMicroelectronics. Full schematics has been included in the Appendices chapter.
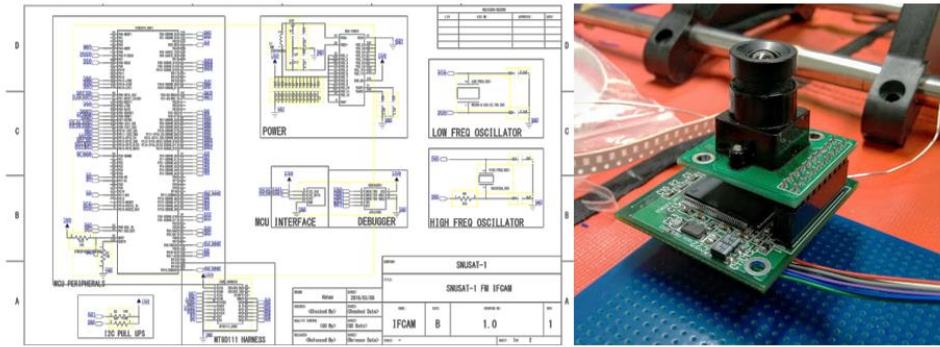
Figure 14 Schematics for IFCAM (Left, refer to appendix), IFCAM V.1 (Right)
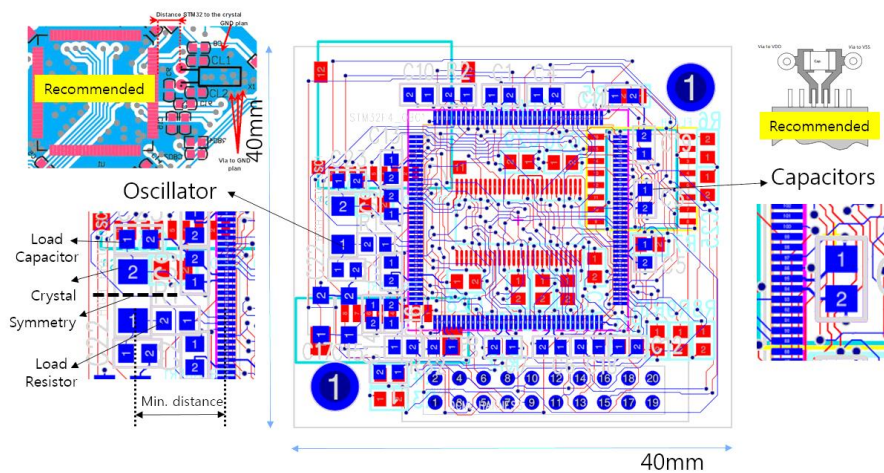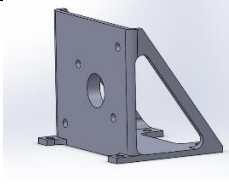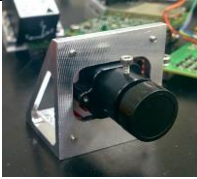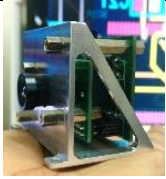
Figure 15 Improvements in design by implementing
recommended layout settings for IFCAM V.1

2.4.5. Structure Design:

Any modular camera requires rigid structure to enclose and hold the PCB. Two structures were built in accordance the requirement specified by SS1-IFCAM-001/002. Both structures exhibit minimalistic design and is focused on minimizing as much physical parts as possible. Rather than opting for a box structure, they are open structured design to minimize weight and manufacturing process. For manufacturing, milling is used to create the structure from a block of Al-6061. The comparison between two structural iteration is provided in the next page.
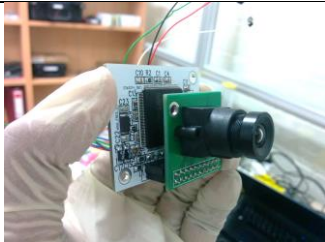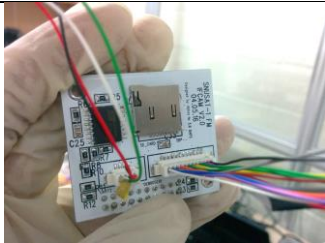
Table 4 Comparison between two structures developed for IFCAM

IFCAM Structure → Parameters		
Structure Version	V1.0	V2.0
CAD	SolidWorks, AutoCAD	SolidWorks, AutoCAD
Volume/ thickness	40 X 40 X 30/ 2 (mm)	55 X 48 X 43 /2 (mm)
Mass	18g + 5g (lens holder)	26g
Material	Al-6061	Al-6061
Lens Holder Type	M12 X 0.5 (black anodized)	M12 X 0.5
Manufacturing Process	Milling	Milling
Lens Holder		Embedded lens holder
Application		
Image Sensor	CP8108	MT9D111
PCB Fit Test		
Overall Mass	<50g	<60g
Modular	Semi (harness: Molex)	Full (harness: Molex)

2.5 Flight Model PCB Design

The following parameters have been selected for flight model based on PCB and structural prototyping as discussed in Chapter 2.4.

Table 5 IFCAM V.2 properties

Top PCB View	Parameters	Properties
	IFCAM Ver.	2.0
	Prototype Model	FM
	Structure Ver.	2.0
	Total Mass	<60g
Bot PCB View	DCMI	8-bit
	IFCAM Connection	UART, I2C, JTAG
	Harness	53261-1271 (Molex)
		53261-0471 (Molex)
	Power Input	3.3V
Sample Image	Power Consumption	<300mW
	Image Module	MT9D111
	Format	RGB565
	Image Resolution	160 X 120 QQVGA
	Binning	2X

3. Software

3.1. Introduction

A set of instructions for the hardware to execute is the software. The software is coded using several layers of library. Higher language library interact with lower language library and that is translated to machine understandable binaries. An Integrated Development Environment (IDE) is responsible for the translation. IDE is a platform that allows users to create a project file which consists of the library and user code. The IDE compiles a "sketch" which is then loaded on to the flash boot memory of the processor. The platform also allows users to debug.

IFCAM utilizes different libraries and software to build the camera instruction software. Libraries such as CMSIS and HAL, and software such as IAR Workbench IDE, SOC 2010 Registry Wizard and STM32CubeMX have been utilized. Details have been provided in the next sub-chapter.

3.2. Software Development Tools/Resources

3.2.1. Integrated Development Environment

An IDE is an application that provides software engineers with a platform to develop embedded software. An IDE normally consists of source code, build automation tools and a debugger. SNUSAT-1 IFCAM uses licensed IAR Workbench 7.4 for ARM for development of IFCAM software.
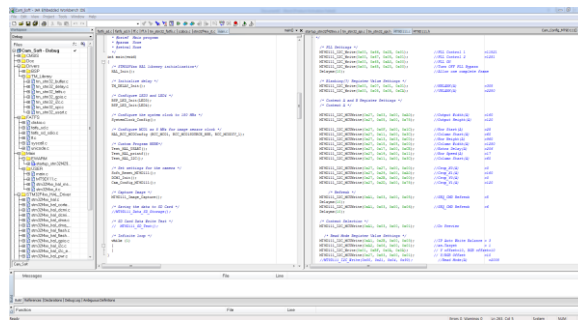
Figure 16 IAR Workbench running on Windows OS

3.2.2. Libraries:

In programming, libraries are non-volatile resources used for developing software. These could include but not limited to pre-written code, sub-routines, classes, documentation, configuration settings and so forth. Libraries usually contain a source (.s) and header file (.h). The source contains the commands or subroutines while the header files have the declares and configurations. Description of libraries implemented are given below:

A. CMSIS: Cortex Microcontroller Software Interface Standard

To bring uniformity in software development of all ARM processors, ARM released ARM Cortex Microcontroller Software Interface Standard (CMSIS). The standard has made migration of software between different ARM Cortex M (0,3,4) easier and has simplified overall software design experience.
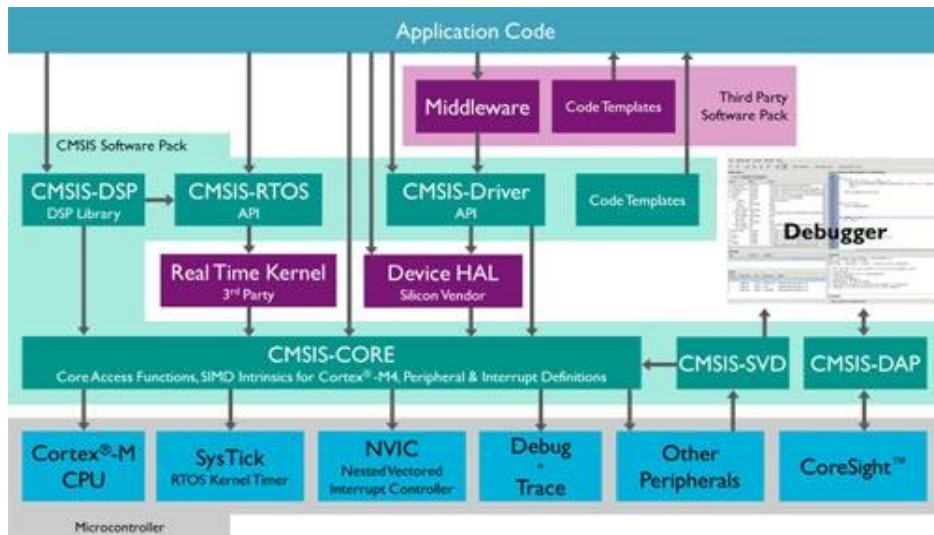
Figure 17 Software layers from high level at the top to low level at the bottom

B. ST Standard Peripheral Library (ST SPL)

The ST SPL provides a set of functions for handling the peripherals on the STM32 Cortex-M4 family. The library allows users to work on a standard, understandable code rather than directly work with registers. Initial software development of IFCAM used ST SPL, however, STM released the Hardware Abstraction Layer (HAL) Library and the IFCAM software was ported to HAL Library.

C. Hardware Abstraction Layer Library (HAL)

STM's HAL library is mature, stable and simpler to use than its predecessor, ST SPL. The library has the same function as the ST SPL and can directly replace ST SPL if porting is done correctly. HAL Library provides a layer of generic multi-instance simple set of Application Programming Interface (API) to interact with the upper layer, i.e. the application, middleware and stacks.
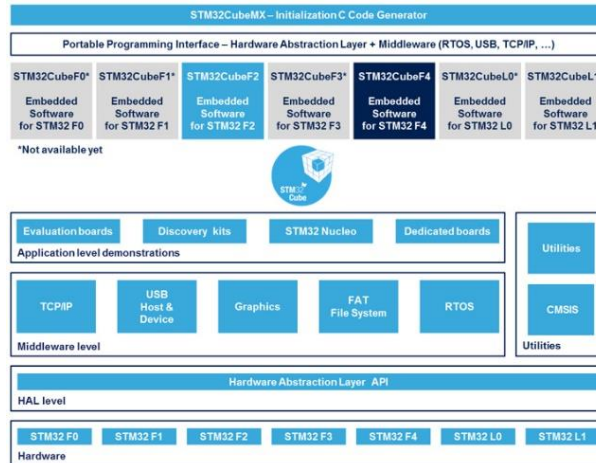
Figure 18 HAL directly interfacing with the hardware

D. FatFs

FatFs is a generic FAT/exFAT file system module for small embedded systems. The library is open source and is useful while integrating non-volatile storage into the camera. Currently, FatFs has been implemented on the SD Card to store images taken by the camera.

E. Tilen Majerle Hardware Abstraction Layer Library (TML)

TML is an open source, ST HAL based library that is well documented and easy to use. TML allows developers to call functions much like how GPIOs are initialized in an Arduino. This upper layer functionality increases prototyping speed and reduces effort in part of the coder. TML has been implemented on Universal Asynchronous Receiver/Transmitter (UART), I2C and FatFs on the camera software.

F. FreeRTOS:

A camera could have simultaneous tasks; check temperature, handle interrupts, power down the camera, run watchdog timer. These tasks can be implemented in the barebone design, however, cameras with a Real Time Operating System (RTOS) could arrange these task and prioritize them. FreeRTOS is a popular open source RTOS. At the time of this writing, however, RTOS has not been implemented on the camera.

G. JPEGLib:

Downlink time has been the limiting factor for image resolution. As mentioned in Chapter 2, a QQVGA image requires at least two passes for image to completely download. One way to obtain high resolution image without multiple passes is to compress the image. JPEG is a very popular lossy compression algorithm that can be implemented for images that are used for display and not for computation. JPEGLib is a free, open source JPEG compression library that can take a bitmap image and convert into .jpeg files.

Currently, the camera software obtains RGB565 data from the camera and stores it into the volatile storage in .dat file. For JPEG library to work, the RGB565 has to be first converted into a BMP file and then converted to JPEG using JPEGLib. While the process is correctly understood, at the time of this writing, no such attempt at implementing the library has been done.

3.2.3. GUI Software

A. STM32Cube

STM32Cube is a Graphical User Interface Software which is aimed at generating initializing code for STM32F processors. A user can select what peripherals to initialize and the speed at which the processor should run. The software will then automatically generate a project file for IAR Workbench for the programmer to start building the software without going through the troubles of writing initializing code. This saves significant time and also guarantees that the processor is running at correct speed.
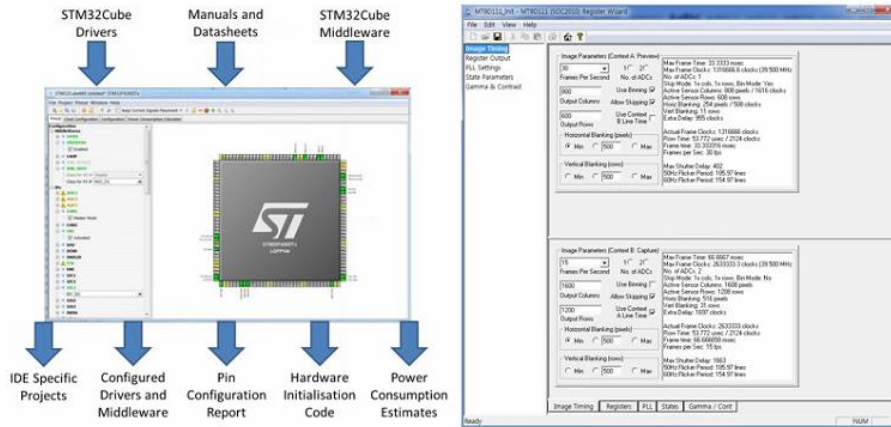
Figure 19 STM32CubeMX software (Left) and SOC2010 Registry Wizard (Right)

SOC2010 Registry Wizard

The SOC2010 Registry Wizard generates registry information for MT9D111. The software allows users to provide information on camera resolution, speed, ADC, binning, auto-exposure, auto-focus and so forth. The registry information can be then coded on to the image sensor using I2C through the processor.

3.2.4. Non-GUI Software

A. FFmpeg

Initially developed for Linux, the software can now be installed on most operating systems including Windows. FFmpeg is an open source software that can handle multimedia files. For IFCAM, FFmpeg is part of the ground testing software. The RGB565 data file acquired can be converted into png file through the software. FFmpeg does not have a GUI interface and instead relies on command prompt.

3.3. Software Description:

There are two versions of IFCAM software; Mission Mode and Ground Testing Mode versions. The basic structure of the algorithm is the same, however, the use of peripherals is different. They have been discussed in details in the following subchapters.

3.3.1. Mission Mode Description
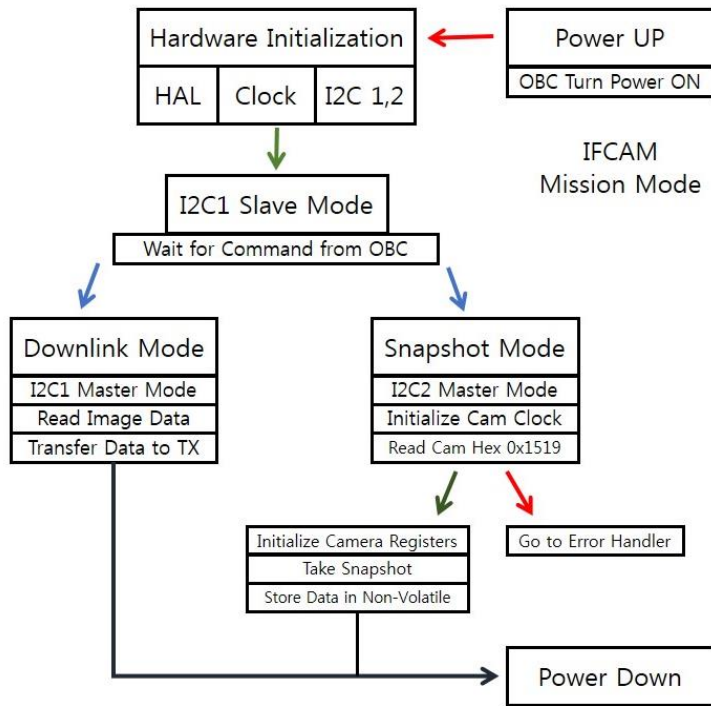
Figure 20 Mission Mode Algorithm

The current version of IFCAM is based on a bare-bone structure. Once the power is switched on by the OBC on the IF3, the processor and camera receives power simultaneously. After stable power supply, the processor initializes all the peripherals including initializing the HAL library, system clock, I2C and DCMI. The I2C1 will then wait for an interrupt from the OBC and according to the hex value, will proceed to either Downlink or Snapshot mode.

For Snapshot Mode (SM), I2C2 master mode will be initialized. I2C2 is interfaced with the MT9D111 image module. The system will then provide a stable 12MHz clock to the camera through Master Clock Output (MCO) and read camera chip version register R0x00:0. The value has to be 0x1519, otherwise the camera is not present. The processor will then soft reset the camera to reset camera configuration registry to default values. Custom registry values are then overwritten on these registries to achieve desired image resolution, camera internal clock speed, pad slew rate among others. After completion, the processor refreshes the image sensor and delays for a complete frame before proceeding to capture image. The image is then

written on the non-volatile storage through SPI.

For Downlink Mode (DM), the processor will control the I2C bus of the satellite. This allows the camera to directly send the data to telemetry. Once the I2C connects with the antenna, the data will be read through the SPI stored into the processor's internal buffer. The buffer data is then sent through I2C to the telemetry where the data is downloaded to the ground station.

3.3.1. Ground Testing Mode Description
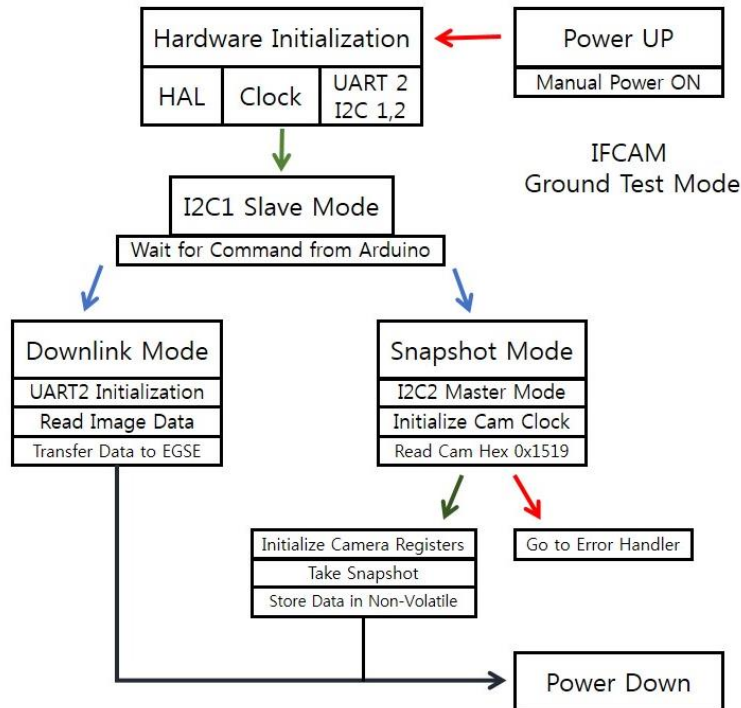
Figure 21 Ground Testing Mode Algorithm

The ground testing mode is similar to the mission mode. The difference is that an Arduino acts as a pseudo-OBC and UART is used to interface with the Electrical Ground Support Equipment (EGSE). The EGSE is connected to the computer through USB2.0. Here, computer acts as the pseudo-ground station. To reduce development time, open source software are utilized to capture RGB565 image. The RGB565 data is sent through the UART to the EGSE which then sends that data to the computer through the USB. The data is captured using serial terminal ComPortMaster from Withrobot Co. The hex values are saved as a .dat file. To check the image, the .dat file is uploaded in www.rawpixels.net website and viewed.

Figure 22 ComPortMaster captures RAW RGB565 hex values

3.3.3. Camera Core Function Description

A. HAL_RCC_MCOConfig ()

After power has been supplied to the camera, a clock signal needs to be provided to the camera. This is done through the Master Clock Output (MCO) 1 of the processor. The MCO is programmed to provide a signal clock of 12MHz which is the same as the external oscillator placed on the MCU.

B. Test_HAL_I2C ()

The I2C is firstly initialized. Then the MT9D111 receives command through the I2C. To verify the camera is MT9D111, the processor reads the version register R0x00:0 to check if the value returned is 0x1519.

C. Soft_Reset_MT9D111 ()

The camera's registry values have to be reset in order to set new configuration. This function resets the sensor through the I2C. No hardware reset is implemented.

38

D. Cam_Config_MT9D111 ()

This function configures Phase Locked Loop (PLL) settings to run the camera at 40MHz, sets auto exposure and target values, changes resolution and waits for the camera to reach In-Preview state.

E. MT9D111_Image_Capture ()

Captures a frame of image through the DCMI and stores it in the local SRAM buffer through the DCMI.

F. MT9D111_Data_SD_Storage()

Stores image data onto SD card using FatFs library. The data is stored as IMAGE_XXXX and automatically increments as new image is stored. A maximum of 10,000 images can be stored.

4. Verification

4.1. Field Testing

Chapter 1 discussed how taking images in earth and from space are similar. To check the performance of the camera in bright and low light conditions, field testing was done from the high grounds of Seoul National University. The engineering building 301 posed an interesting option to take long distance, infinity focused images. However, initial test results showed that saturated, plain white images. The exposure setting on the camera worked indoors but performed poorly outdoors during bright daylight.

Figure 23 Outdoor testing on building 301 at Seoul National University (SNU) at Gwanak Campus. Testing equipment included EGSE, IFCAM and laptop.

The camera responded later during sunset, and the following images were captured in QQVGA format.

Figure 24 Initial outdoor results taken at 19:31, 19:36 and 19:41 by IFCAM

Results showed that a NIR filter was required for the lens and that the both the White Balance (WBS) and Exposure Settings (ES) were not working as initially thought.
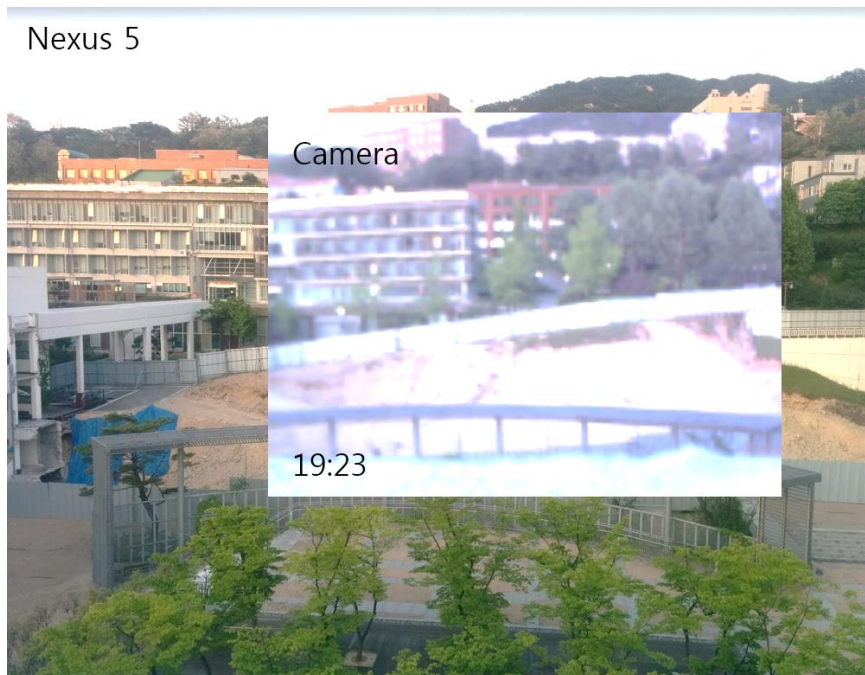
Figure 25 Improved image taken at 19:31. The higher resolution image is taken by Nexus 5 phone while the lower resolution image is taken by IFCAM.

A stock lens (f# not provided) with NIR cut-filter was used to take another image during a similar time. The result shown in Fig. 25 shows significant improvements on the color, brightness and WB of the image.

Nexus 5   Camera
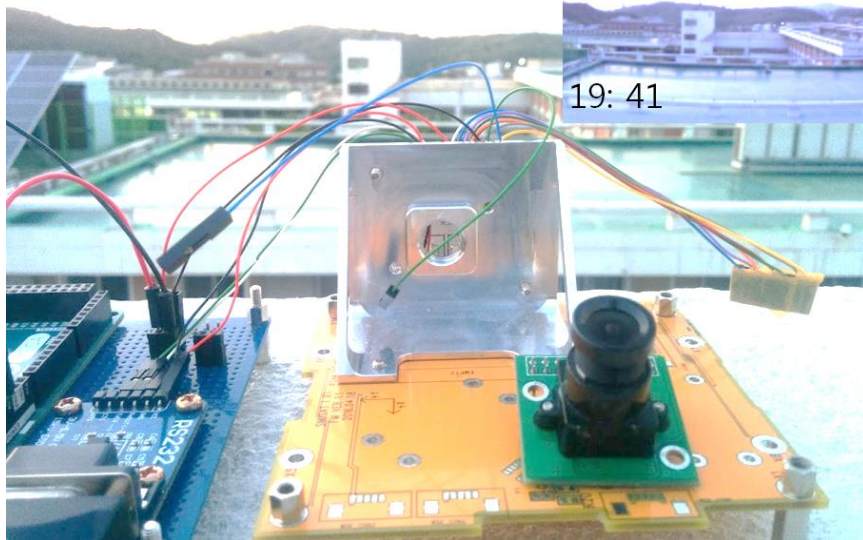
Figure 26 Far field testing with IFCAM at 19:41.
Comparison is made through picture taken by Nexus 5 phone and IFCAM.

For far field testing, the camera was placed such that it would take image of the sky, hills and the foreground consisting of buildings in SNU. The camera performed better after the sun had set, exposing the need to improve the software for ES and WBS.

4.2. Vibration Testing

4.2.1. Introduction

A payload inside a launcher is subject to severe vibration during launch phase. Vibration tests on the payload which simulate the environment inside the launcher is useful in determining the structural integrity of the payload. The goal of vibration testing is to simulate the launch environment in a laboratory environment. Although technically difficult to achieve, the testing should accurately reproduce the dynamic condition inside the launcher. A payload's integrity can be positively determined if the testing is accurate.

4.2.2. Types of vibration testing

Vibration testing include Random Vibration Test (RVT), Sine Vibration (SV), Sine Burst (SB) and Shock Testing (ST). The IFCAM was tested using the RVT while taking calculated risk not to undergo SV, SB and ST. A better understanding of why RVT was chosen has been discussed below.

4.2.3. Random Vibration Testing

RVT excites Device Under Test (DUT) at all frequencies at a given bandwidth. The bandwidth typically ranges from 20Hz to 2000Hz. At each frequency, the energy is controlled at a specified level. The actual amplitudes are random with a Gaussian distribution around desired test level [Wilson, 1989, p.1]. Generally, RVT is an accepted method of generating many actual dynamic environment during an actual launch [Wilson, 1989, p.1]. This is why RVT is the dominant method of testing for vibration.

In practice, DUT is not excited in all frequencies inside the bandwidth. Rather, the frequencies are grouped into discrete chunks called frequency bandwidth. The selection of frequency bandwidth is dependent upon the vibration control system and the operator. Amplitude levels are normally specified in units of G^2/Hz (Reference) where the Hz unit is in reference to filter bandwidth.

One of RVT's primary objective is to verify the strength of secondary structures like DUT housing, electronic boards and fixing structures. This builds confidence in general integrity for structures including small solder joints, fasteners and electrical connectors. Additionally, the cyclic stress that RVT imposes on the DUT provides a good understanding of the structure's resistance to fatigue, although the test procedure should be different for different class of test. Engineering Qualification Model (EQM) undergo more stringent, longer testing than Flight Model which undergo a test set at the typical Maximum Predicted Environment (MPE). The DUT for IFCAM was an EQM, however, the test was placed under MPE as the IFBATT (Interface Battery), which was being tested together, was undergoing Acceptance Test (AT) for IFBATT's FM.

4.2.4. Instrumentation and Fixtures for RVT

The primary component for RVT is the electrodynamic shaker as shown in Fig. 27. The shaker can produce any vibration profile from 5Hz to 25000Hz and is only limited to its peak acceleration, velocity and displacement. The electrodynamic

shaker is controlled by digital system which incorporates Analog to Digital Converters (ADC)/Digital to Analog to Digital Converters (DAC) hardware, multipurpose computer and a high speed co-processor to achieve vibration control. Software running on these digital system double as both an interface for engineers to create random vibration profile and control the shaker, and also to analyze raw data.
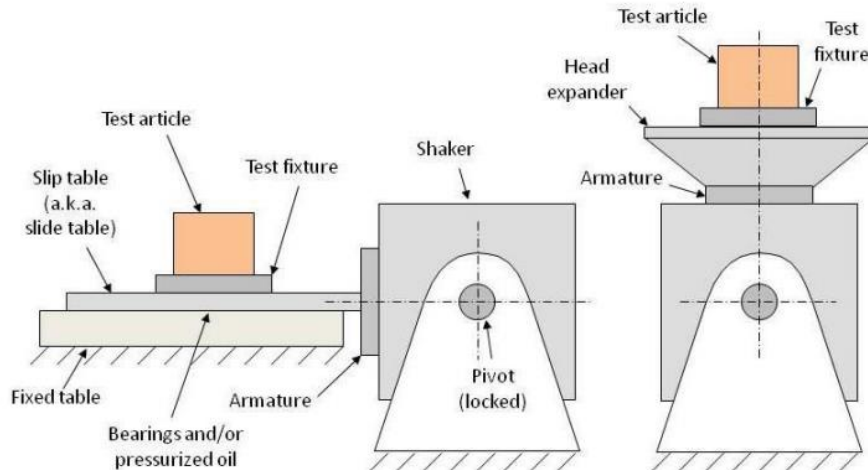
Figure 27 Electrodynamic shaker test setup for X/Y axis (L) and Z axis (R)
[Sarafin et al, 2014, p.2]

Real-time acceleration data is acquired through accelerometers placed on the DUT and the shaker. An accelerometer is an instrument that measures the acceleration indirectly from deformation, which in turn relates to inertia force that resists acceleration [Sarafin et al, 2014, p.7]. Two common type accelerometers are piezoelectric (PEA) and piezo-resistive accelerometers (PRA), however, PEA are used for RVT. This is because PRA are sensitive to high frequency and RVT can go up testing can go up to 2kHz. As mass accelerates, the amount of deformation that the DUT is undergoing correlates to the acceleration of the body. A calibrated PEA can thus, accurately measure the acceleration. PEA measures alternating acceleration and not steady state acceleration, and is therefore, not recommended for low frequency testing <2Hz. Since RVT ranges from 5Hz-2000Hz, PEA is selected for RVT.

The DUT has to be firmly fixed on to the electrodynamic shaker. A fixture called a *jig* interfaces the DUT to the shaker. A reasonable compromise has to be made while designing the jig such that the fixture is stiff enough but does not influence the natural frequency of the DUT.

4.2.5. Actual Testing

The DUT (IFCAM) underwent the following tests in each X, Y, and Z axes.

- Resonance Survey
- RVT

A. Reference Test

The following tests were performed for the DUT before and after vibration testing between each axis of vibration.

- Image Blur Test
- De-soldering Inspection Test

B. Pass/Fail Criteria

Visible deformation of soldering that lead to loss in electronic components and visible blurring of images taken after each axis vibration by the camera will categorize DUT as failure.

C. Configuration Items

The configuration items of the vibration test campaign consisted of DUT, base jig, accelerometer, electrodynamic shaker and electronic components related to shaker.

D. DUT

IFCAM along with InterFace Battery (IFBATT) were tested together. 4 IFBATT PCBs were stacked on top of each other and then the IFCAM was stacked on top of the 4 IFBATT PCB. The IFCAM was fixed to IF1 (Interface Board 1) dummy PCB.

Socket head Cap M3 screws, spring spacers and nuts were used to fix the IFCAM processor PCB, image sensor PCB and IFCAM structure together. SUS spacers 5mm and 20mm were used. A torque of 2.48Nm was used to fix each M3 screw. The same screws were used to fasten the IFCAM structure to IF1 PCB. To confirm fixing, 3M Scotch-Weld Epoxy Adhesive EC-2216 Gray epoxy was used where the screws/bolts came in direct contact with the IFCAM structure. The M12 X 0.5 lens was also fixed to the structure using the same epoxy.

E. Base Jig

A base jig is designed to decouple the jig natural frequency from the testing frequency range. In order to ensure this, the thickness of the jig is designed to be 50mm using AL7075. The base jig is show in the figure below
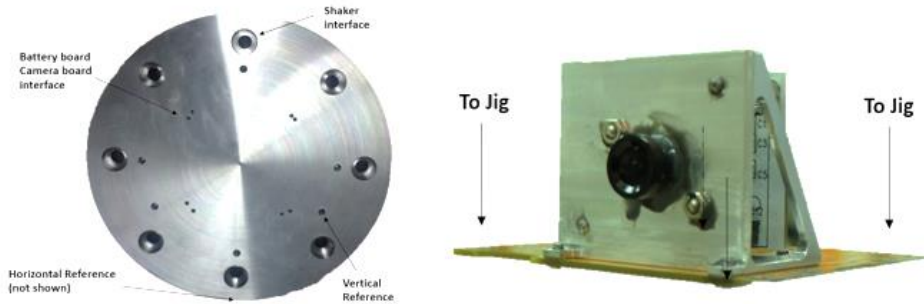
Figure 28 Jig (L) with how IFCAM was fixed to the Jig (R)

There are six threaded holes for vertical reference accelerometers with two threaded holes for horizontal reference accelerometers. The battery board interfaces in two directions, in order to reduce the need to disassemble jig when changing the axes between X and Y.

F. Accelerometers

Accelerometers are used to measure the acceleration level of the control and response of the DUT. In order to do so, accelerometers are attached on the jig as reference and on the IFCAM. The attached positions are shown in the figure below:
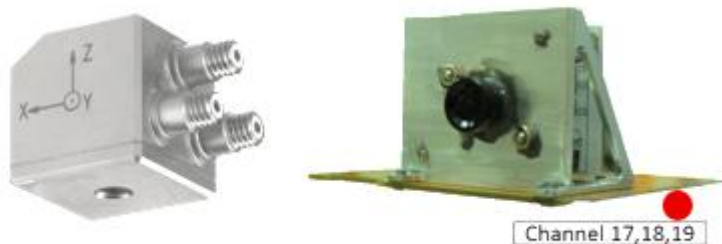
Figure 29 Example of a 3-axis accelerometer (R) and placement of the accelerometer on IFCAM mounted on IF1

Table 6 Accelerometers associated with IFCAM during testing

Sensor ID	Component	Position	Direction
Channel 17	IFCAM	Top right corner	Y
Channel 18		of bottom side of	Z
Channel 19		PCB	X

G. Experimental Apparatus

This section lists the experimental apparatus used throughout the IFCAM vibration testing. The experimental apparatus used are listed in the table below.

Table 7 Test components

Apparatus	Model	Description
Shaker	LING 1216VH	Shaker used for vibration test procedure
Camera	Canon	Used for visual inspection
EGSE	IFCAM EGSE	Interface computer and provide power to IFCAM
Computer	Samsung	Download and store image data

Figure 30 Images taken during RVT at SaTRec facilities, KAIST, Daejon

H. Shaker

Model information is as follows:

- Model 1216VH Electrodynamic Shaker (Ling Electronics, USA)
- Model DMA1212E Power Amplifier (Ling Electronics, USA)
- Vibration Shaker Control System with Jaguar (Spectral Dynamics, USA)

Table 8 Shaker information

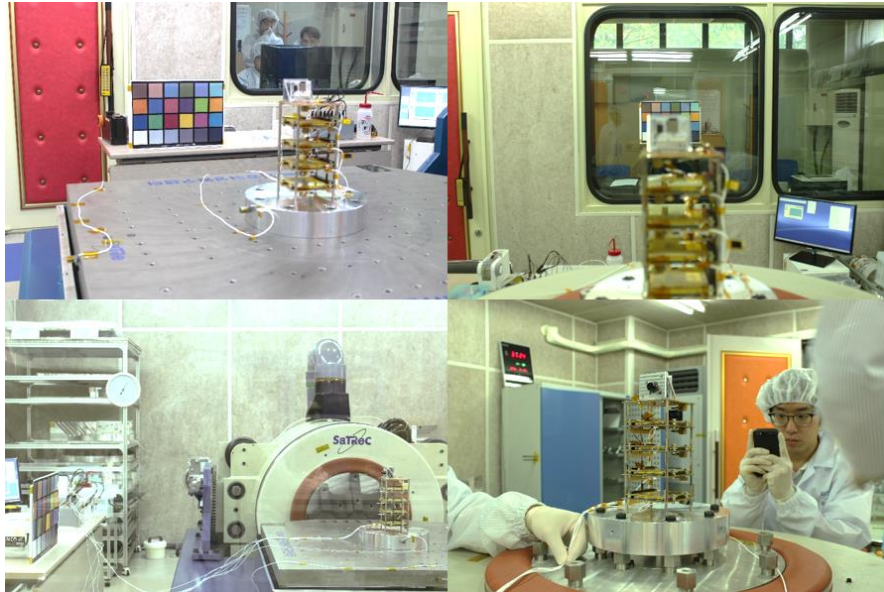| Item	Specification
Force Rating	12,000 lbs. (53.4kN) peak sine, 12,000 lbs. (53.4kN) RMS random, 24,000 lbs. (106.8kN) Shock
Maximum Acceleration	100g sine vector
Displacement	1.5 in.p-p(38.1mm) continuous, 2.0 in.p-p(50.8mm) shock, 2.2 in.p-p(55.9mm) between mechanical limits
Maximum Velocity	70 IPS (1.78m/s), bare table as limited by Amplifier voltage
Frequency Range	5~3000 Hz
Fundamental Axial Resonance	2260 Hz (nominal)
Armature Weight	120 lbs. (54.4kg)
Armature Suspension	Half-loop metallic flexures
Axial Stiffness	440 lbs. per inch (77kN/m)
Vertical Load Support	1500 lbs. (680kg) standard
Armature Diameter	17.25 in. (438mm) with 16" bolt pattern
Cooling	Air-cooled by suction-type 20Hp blower; blower to shaker flexible air duct

I. Bolting

During the test, bolting was required while interfacing the IFBATT/IFCAM board(s) with the jig and the jig with the shaker. The list of the bolts and recommended assembly torque which were applied are given in the Table 9.

Table 9 Bolting fixture information

Material	Standard	Torque Nm
SUS	M3	0.63
	M10	24.5
SCM	M3	1.14
	M10	44

J. Resonance Survey

Resonance survey was conducted in order to identify the characteristics of DUT. The survey is conducted before and after each of the vibration tests. An initial survey before RVT will identify dominant modes of the DUT. Repeating the same survey after DUT has gone under RVT should produce the same profile, otherwise any shift in the resonance amplitude or frequency should indicate damage to the equipment. For instance, a simple shift in natural resonance frequencies might suggest a few loose bolts (Baren, 2012).

Table 10 Sweep rate and resonance profile for survey

Sweep rate	4 oct/min	
Profile	Frequency [Hz]	Amplitude [g]
	5	0.15+
	2000	0.15+

K. Random Vibration

RVT is the main vibration test for IFCAM. RVT is performed for each of vibration axes (X, Y, Z). Image is taken before and after RVT in each axis. The spectrum is shown in Table 11.

Table 11 Random Vibration profile

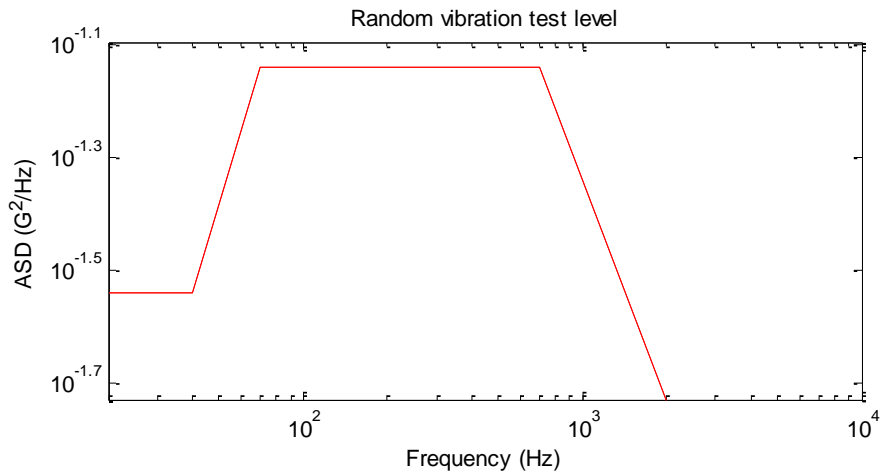| Frequency (Hz)	ASD (G^2/Hz)	dB/OCT	G$_{rms}$
20.00	0.028800	*	*
40.00	0.028800	0.00	0.76
70.00	0.072000	4.93	1.43
700.00	0.072000	0.00	6.89
2000.00	0.018720	-3.86	9.65

Figure 31 RVT test envelope

L. Vibration Test Sequence

The overall vibration test sequence is shown in table below

Table 12 Resonance survey test profile

No.	Vertical/Horizontal	Axis	Vibration	Frequency [Hz]	Test duration [s]
1	Horizontal	Y	Resonance	5-2000	260 (4 oct/min)
2	Horizontal	Y	Vibration	20-2000	60
3	Horizontal	Y	Resonance	5-2000	260 (4 oct/min)
4	Horizontal	X	Resonance	5-2000	260 (4 oct/min)
5	Horizontal	X	Vibration	20-2000	60
6	Horizontal	X	Resonance	5-2000	260 (4 oct/min)
7	Vertical	Z	Resonance	5-2000	260 (4 oct/min)
8	Vertical	Z	Vibration	20-2000	60
9	Vertical	Z	Resonance	5-2000	260 (4 oct/min)

4.2.6. Results

A. Resonance Survey

<p align="center">X-Axis</p>
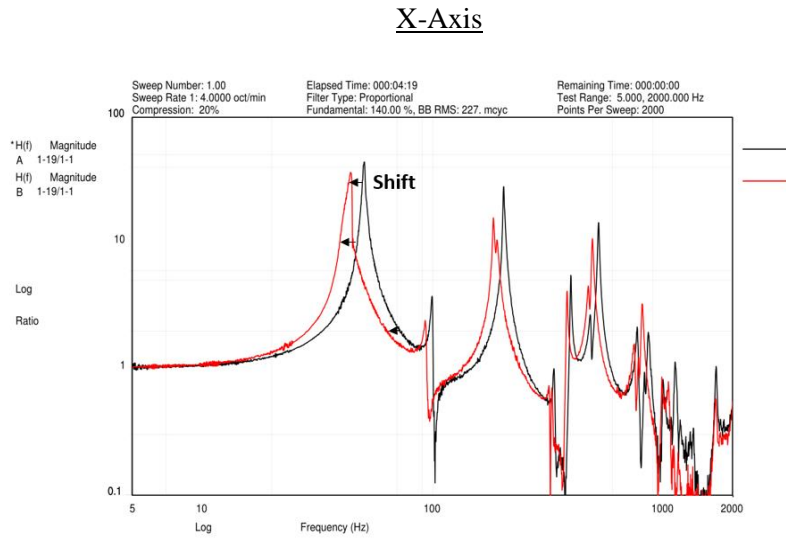

Figure 32 Resonance survey for X-axis shows shift in the modes. The magnitude and frequency are both given in logarithmic scale.
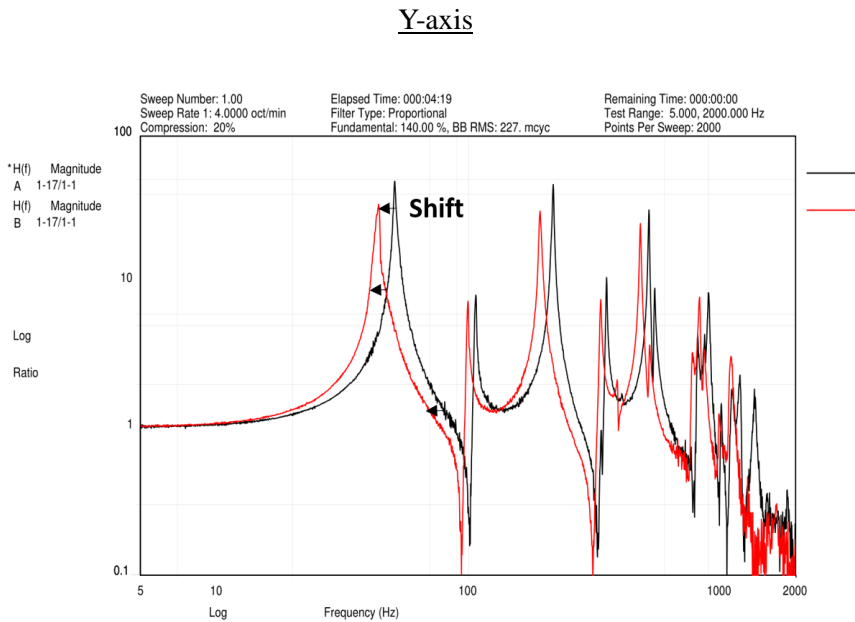
<p align="center">Y-axis</p>

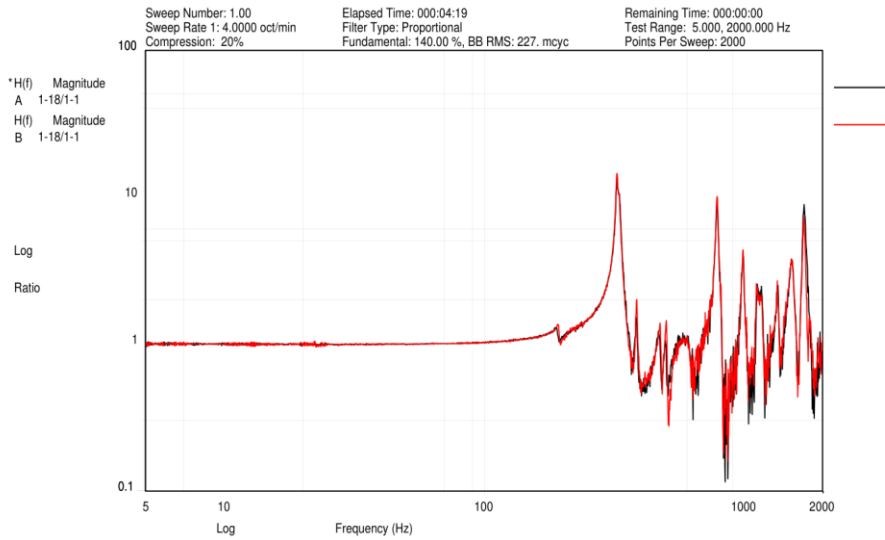**Figure 33** Resonance survey for Y-axis shows shift in the modes

Z-Axis

Sweep Number: 1.00   Elapsed Time: 000:04:19   Remaining Time: 000:00:00
Sweep Rate 1: 4.0000 oct/min   Filter Type: Proportional   Test Range: 5.000, 2000.000 Hz
Compression: 20%   Fundamental: 140.00 %, BB RMS: 227. mcyc   Points Per Sweep: 2000

*H(f)   Magnitude
A   1-18/1-1

H(f)   Magnitude
B   1-18/1-1

Log

Ratio

Figure 34 Resonance survey of Z-axis shows no shift

B.   RVT

X-Axis

Test Level: 0.000 dB   Reference RMS: 9.654   Test Range: 20.000, 2000.000 Hz
Test Time: 000:01:00   Clipping: Off   Resolution: 0.625 Hz

*Control
A
Auxiliary   7
A
Auxiliary   13
A
Auxiliary   19
A
[Log]

g?Hz
DOF 120
RMS:
9.616 g
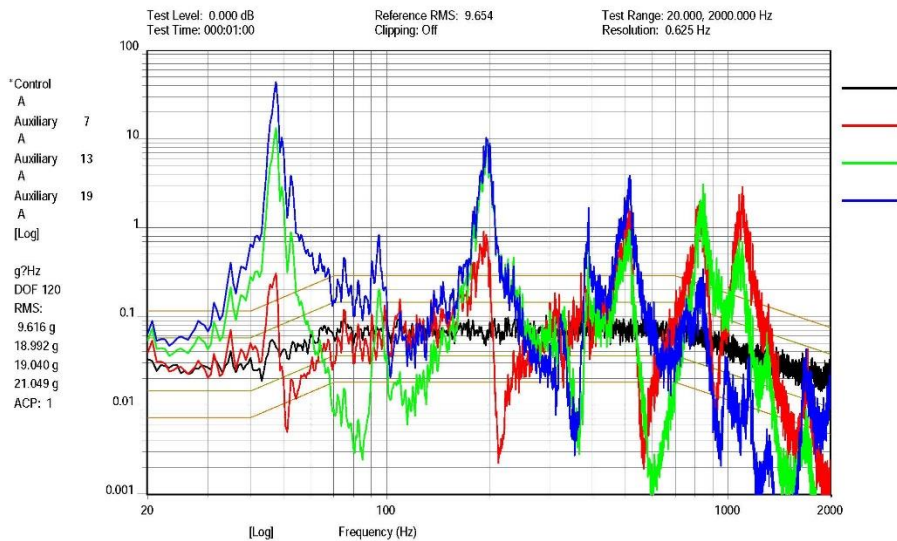18.992 g
19.040 g
21.049 g
ACP: 1

Figure 35 IFCAM's response highlighted in blue and Ch.19
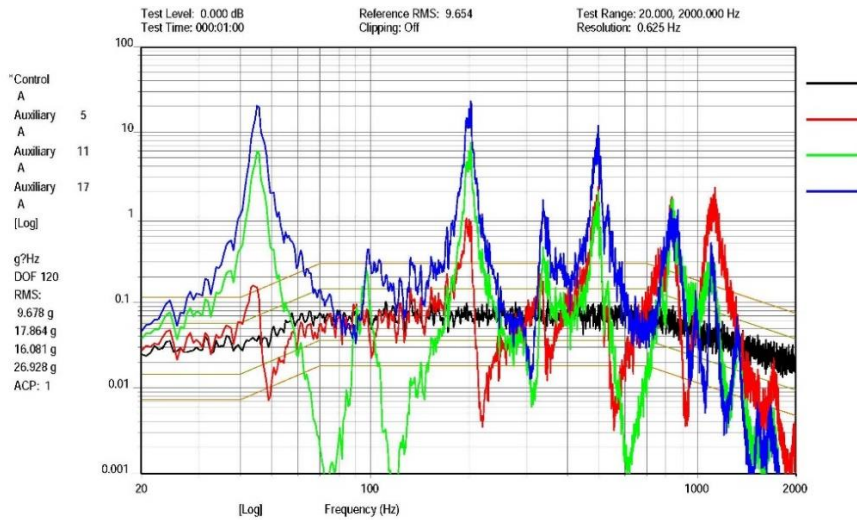
52

Y-Axis

Figure 36 IFCAM's response highlighted in blue and is Ch.17
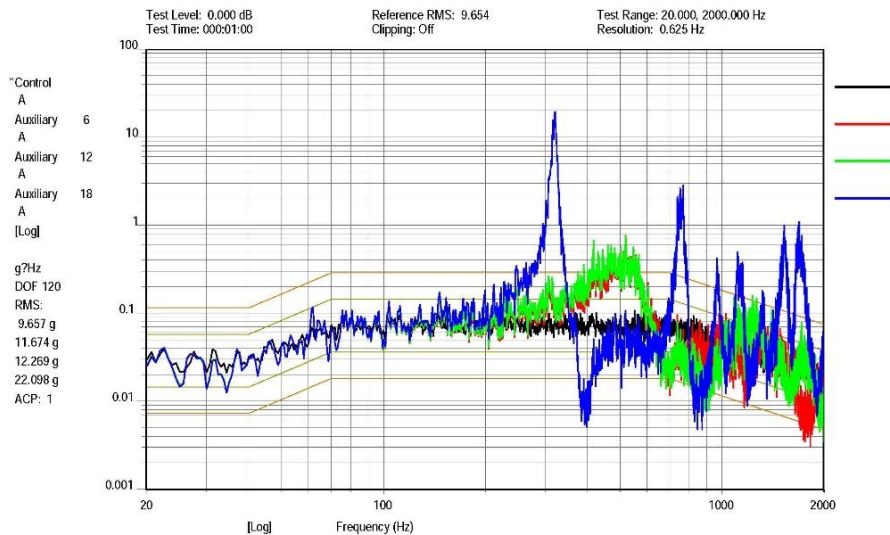
Z-axis

Figure 37 IFCAM's response is highlighted in blue and is Ch.18
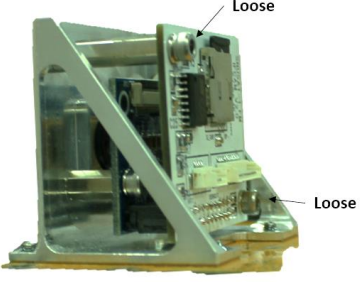
4.2.7. Result discussion

Summary of the data is provided below in Table 13.

Table 13 Modal survey summary for X, Y and Z axis for IFCAM

Sequence (Channel)		Ref	FRF @ Natural Frequency	Remarks
X (19) →	1	Modal Survey 1	43.85 @ 50.416Hz	Ref=0.15g(5~2000Hz)
	2	Random Vibration (0dB)	21.049 G_{rms}	Control: 9.616 G_{rms}
	3	Modal Survey 2	36.31 @ 44.055Hz	Ref=0.15g(5~2000Hz)
Y (17) →	1	Modal Survey 1	48.75 @ 51.024Hz	Ref=0.15g(5~2000Hz)
	2	Random Vibration (0dB)	26.928 G_{rms}	Control: 9.678 G_{rms}
	3	Modal Survey 2	33.96 @ 43.923Hz	Ref=0.15g(5~2000Hz)
Z (18) →	1	Modal Survey 1	13.21 @ 323.30Hz	Ref=0.15g(5~2000Hz)
	2	Random Vibration (0dB)	22.098 G_{rms}	Control: 9.657 G_{rms}
	3	Modal Survey 2	14.42 @ 322.33Hz	Ref=0.15g(5~2000Hz)

The data shows that IFCAM was able to withstand a RVT of 26.928G_{rms} in the Y-axis, 21.049 G_{rms} in the X-axis and 22.098 G_{rms} in the Z-axis without undergoing deformation. The modal survey on X and Y axis showed that the modes had shifted to the left, and the explanation has been provided in Page 55. The test condition for RVT was set to 0db which is the MPE. The RVT at MPE was given to be 9.65 G_{rms} which is smaller than what the IFCAM withstood in all the axis. Modal survey for both X and Y axis showed that there was a shift of resonant modes towards the left. As explained before, deformation or loosing of bolts could have been one of the reasons. A visual inspection was made to find the issue

Table 14 Visual Inspection to understand why the modes shifted

	IFCAM Components	Visual Inspection Remarks
Loose (image label) / Loose (image label)	SMD components	Intact
	IFCAM to IF1 fixture	Intact (epoxied)
	Image board to structure	Intact
	Processor board to structure	Bolts loose for both X and Y axis
	Deformation on structure	Not visible
	Deformation on spacers	Not visible
	SD card	Intact
	M12 optics	Intact

Visual inspection of the DUT showed that bolts holding the IFCAM structure and the processor PCB were slightly loose. One explanation is that the DUT had undergone the highest RVT as the DUT was placed on top of 4 IFBATT PCB which were also DUT. The test condition for IFCAM was, therefore, higher than the MPE. To ensure that the bolts stay intact however, the Flight Model (FM) of IFCAM will have all the bolts epoxied to the PCB.

Figure 38 Top two images are before and after image in their original resolution. For visual inspection both the images were enlarged as shown at the bottom.

Figure 39 Shows cropped image of the ColorChecker Chart for image taken before and after the test. The third picture is the result of the comparative analysis done between the two images.

Visual inspection on the image after X-axis RVT showed no difference on the image. Resemble.js written in HTML5 canvas and JavaScript created by James Cryer was used to quantify the difference. Each pixel from the cropped image is analyzed on the R, G and B channel. Any difference found between the two corresponding pixel from corresponding "before" and "after" is then highlighted by placing yellow color over the pixel. The software showed a difference of **<3.13%**.

Figure 40 Top two images are before and after image in their original resolution. For visual inspection both the images were enlarged as shown at the bottom.

Figure 41 Shows cropped image of the ColorChecker Chart for image taken before and after the test. The third picture is the result of the comparative analysis done between the two images.

Visual inspection on the image after Y-axis RVT showed no difference on the image. Resemble.js was used for analysis and showed that the difference was **<2.34%**.

Figure 42 Top two images are before and after image in their original resolution. For visual inspection both the images were enlarged as shown at the bottom.

Figure 43 Shows cropped image of the ColorChecker Chart for image taken before and after the test. The third picture is the result of the comparative analysis done between the two images.

Visual inspection on the image after Z-axis RVT showed no difference on the image. Resemble.js was used for analysis and showed that the difference was **<2.76%**.

4.3. Vacuum Testing

DUT is placed under a vacuum chamber to check for functionality in vacuum condition

4.3.1. Pre-Vacuum Testing:

Pre-vacuum test is required to set a reference for the vacuum test. Both physical (mass) and image quality were measured. The pre-vacuum test procedure were:
1. Measurement of mass with 0.1g precision
2. Take image

4.3.2. Vacuum Testing:

Post-vacuum test is required to check what difference the vacuum cycle had on the physical and electronical components of DUT. The post-vacuum test procedure were:
1. Measurement of mass with 0.1g precision
2. Take image

4.3.3. Vacuum Cycle:

The vacuum cycle requires vacuuming at 8psi/minute (55,160 Pa/min) down to 0.1 psia (689 Pa or 5.16 Torr) maintained for 6 hours. Re-pressurize procedure required 9 psi/minute (62,100 Pa/min). The example of the vacuum cycle profile is given below:
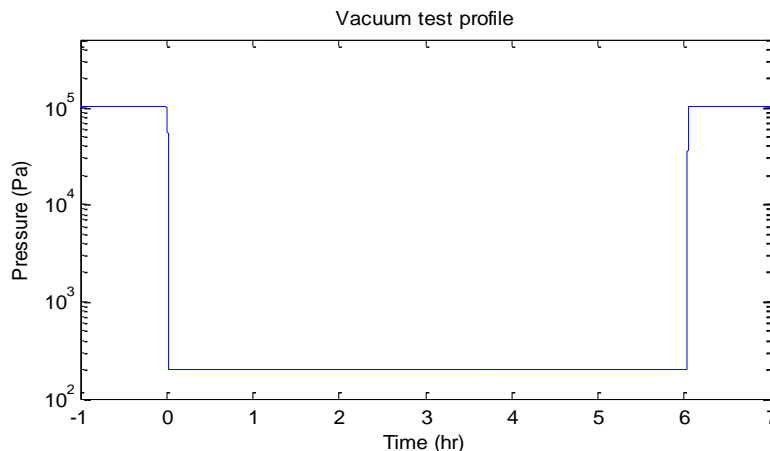

Figure 44 Vacuum test profile shows that the test will be conducted for 6 hours

4.3.4. Experimental Apparatus

This section lists the experimental apparatus used throughout the IFCAM vibration testing. The experimental apparatus used are listed in the table below.

Table 15 Test equipment for VT

Apparatus	Model	Description
Vacuum Chamber	SaTRec TVAC	Chamber used for vacuum test procedure
Camera	Canon	Used for visual inspection
EGSE	IFCAM EGSE	Interface computer and provide power to IFCAM
Computer	Samsung	Download and store image data

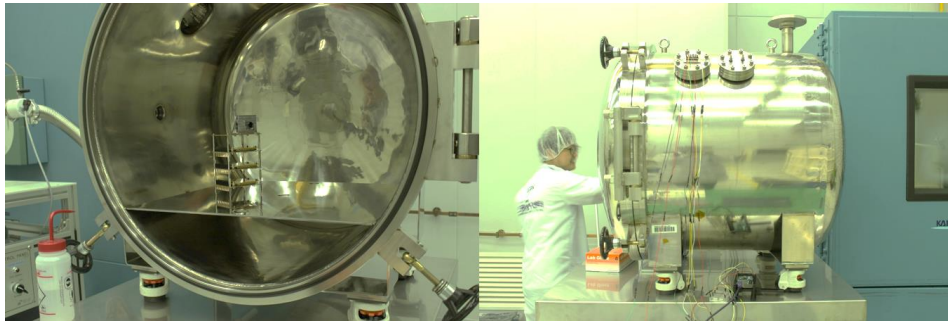**Figure 45** VT test setup at SaTRec, KAIST, Daejon
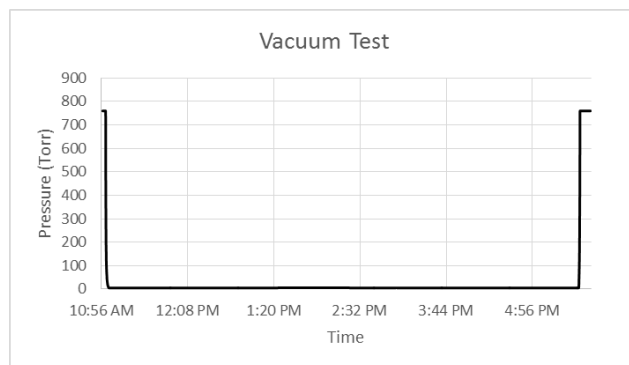
4.3.5. Results

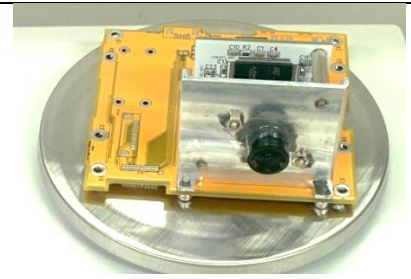**Figure 46** VT actual test profile provided by SaTRec.

The test began at around 11a.m. and ended at 5:30 p.m. The total time was 6.5 hours

One complete vacuum cycle of about 6 hours was made. The results are presented below:

<u>Outgasing</u>

Outgasing is the release of gas that was dissolved, trapped or absorbed in the material. Outgassing can be particularly important to components that directly deal with light. Gas molecules from surrounding materials could eject and stick on the surface of solar panels, reducing its efficiency. A similar case could be made with image sensors.

Table 16 Checking mass of the IFCAM mounted on IF1
before and after the vacuum testing

Measurement	Before (g)	After (g)
	94.19	94.18

Measurement showed a decrease of 0.01g in mass. Outgassing from the DUT was present but is neglegible.

To check the performance of the camera and to see if the outgassing had any apparent effect on the optics/image sensor, visual comparision was made between the image taken before and after the test.
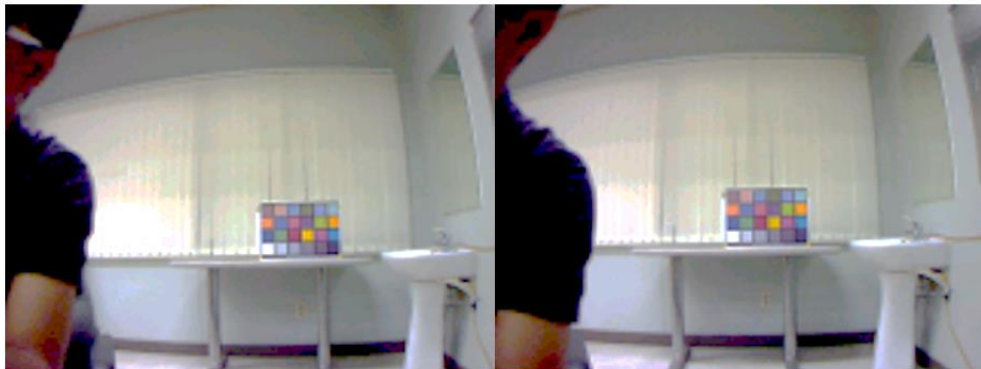
Image Inspection

Figure 47 Top two images are before and after image in their original resolution. For visual inspection both the images were enlarged as shown at the bottom.

Figure 48 Shows cropped image of the ColorChecker Chart for image taken before and after the test. The third picture is the result of the comparative analysis done between the two images.

Visual inspection on the image after Z-axis RVT showed no difference on the image. Resemble.js was used for analysis and showed that the difference was **<1.51%**.

5. Improvements

5.1. Software

Field testing done on Chapter 4 also showed the need to lower the brightness of the image as day time images were saturated. When the camera resets, the datasheet showed that the Auto-Exposure (AE) bit in the mode register is "1" which means that AE is enabled. However, since the test results showed saturated images, the target brightness settings has to be lowered (On Semi, 2007, pg.45) in order to obtain clear image.

The relative EV value can be calculated by

$$\text{Relative EV} = \text{LOG}\left(\frac{ae.Target}{reference\ ae.Target}\right)/\text{LOG}(2) \qquad (3)$$

Where,
ae.Target = new AE target value
reference ae.Target = old AE target value (in this case, the default)

The datasheet explains that in default, the *ae.target* value is set at 60. When a target value is reduced 10, the relative EV value is -2.6.
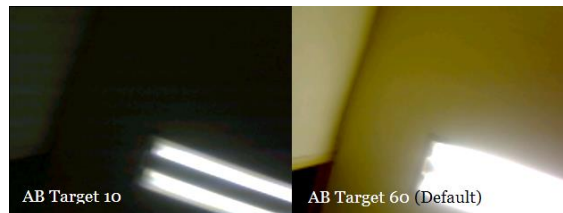

Figure 49 Auto Brightness (AB) or AE comparison between
relative EV -2.6 and EV 0

Figure 50 Another Auto Brightness (AB) or AE comparison between
relative EV -2.6 and EV 0

For outdoor conditions, since the default *ae.target* was 60 and the image was saturated, the *ae.target* had to be chosen between 10 to 60. To reduce the relative EV by -1, the *ae.target* was set at 30.

5.2. Hardware

Field testing verification showed the need for optics to have an IR cut-off filter. The image sensor, MT9D111, has a quantum efficiency of about 17%~19% at 820nm of the electromagnetic spectrum. Without an IR cut-off filter, the RGB bayer filter of the sensor was allowing light above 600nm, specifically around 820nm where the sensor is sensitive to.

To solve this problem, the optics had to be changed to improve the results. Instead of relying on www.devicemart.co.kr where previous COTS S-mount lens was purchased, lens from Edmund Optics was selected as the company has a supply base in Korea. The company's M12X0.5mm S-mount lens was also used in imaging payload system in EstCube1 [Kuuste et al., 2014]
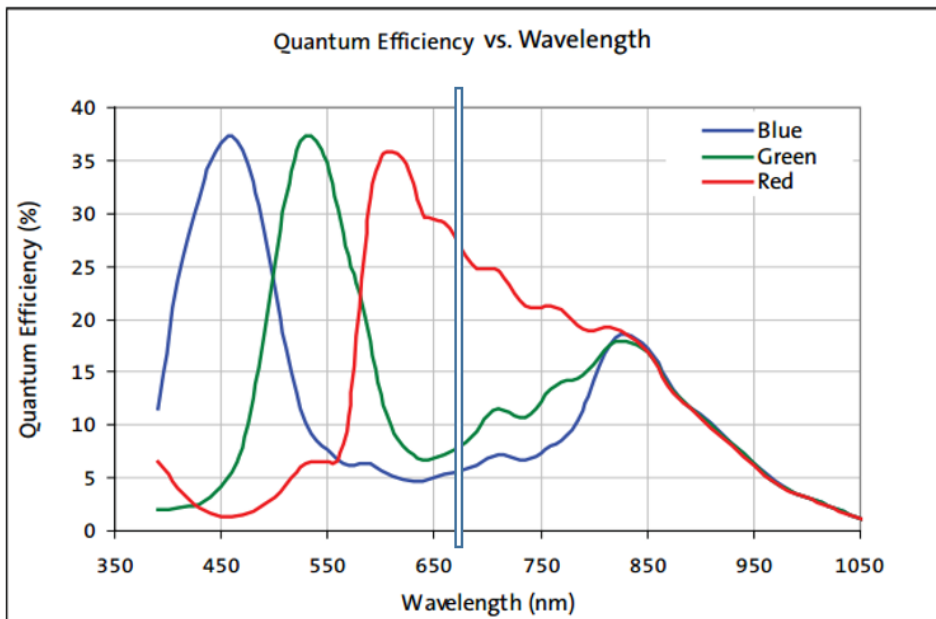

Figure 51 MT9D111's spectral sensitivity given in quantum efficiency.
An IR-cut-off filter is required to avoid the 820nm sensitive peak.

Table 17 Shows comparison of new S-mount lens from Edmund Optics.
The calculation were made for a satellite at 350km orbit

Lens → Parameters		
Focal Length (mm)	3.94	3.0
GSD (m)	497.5	653
GS (km)	401 x 303	572 X 399
IR Cut-Off (nm)	650	650
Aperture (f/#)	f/2	f/2
FOV	74°	97.8°
Max Sensor Format	1/3"	1/3"
Distortion (%) @ Full Field	-29	-52.1
Working Distance	400 - ∞	400 - ∞
Resolution, On-Axis (lp/mm) @ 20 Contrast	88	97
Resolution, 0.7 Field (lp/mm) @ 20 Contrast	54	62
Resolution, Full Field (lp/mm) @ 20 Contrast	46	35
Maximum Diameter (mm)	14.0	14.0
Length (mm)	16.0	15.3
Mount	M12 X 0.5	M12 X 0.5
Type	Fixed Focus	Fixed Focus
Availability	Out of Stock	In Stock

Figure 52 Comparative image between images without IR filter (top)
and with IR filter (bot)

Visual inspection of comparative images taken on top of 301 engineering building showed significant improvements on the color.

65

6. Conclusion

6.1 Requirement review

6.1.1. SS1-IFCAM-001

Requirement stated that the total mass of the system should not exceed 100g. Table 5 showed that the IFCAM, with the structure, weighed less than 60g.

6.1.2. SS1-IFCAM-002

Requirement stated that the volume should remain under $60 \times 50 \times 50$ mm^3. Table 4 shows that the $55 \times 48 \times 43$ mm^3 for the structure. However, this does not take into consideration the extrusion of lens barrel.

6.1.3. SS1-IFCAM-003

Power consumption has to be under 500mW. The current measured for IFCAM was <100mA. The voltage supply is 3.3V and therefore, the power consumption can be calculated as:

$$P = I \times V \quad (4)$$

Where,
P = Power
I = Current
V = Voltage
The power can be calculated as 330mW. This value is the maximum value and is usually consumed while taking an image.

6.1.4. SS1-IFCAM-004

SS1-IFCAM-004 states that the GS should at least cover South Korea which has an approximate area of 400×300 (km). In order to cover that, the lens from Edmund Optics used has a GS of 572×399 (km) Table 16.

6.1.5. SS1-IFCAM-005

SS1-IFCAM-005 states that the design should be modular. The schematics of the camera has been modified and re-implemented on the On-Board Computer of SNUSAT-1. The layout has been shown on Fig. The processor, STM32F49ZI is a feature rich processor as shown on Table XX, has its own Pulse Width Modulation channels for 3-axis Magnetorquer and Analog to Digital (ADC) for analog sensor inputs (thermistors, current sensors, voltage sensors) [Maskey et al., 2016]. The schematics of OBC has been provided in the Appendix section.
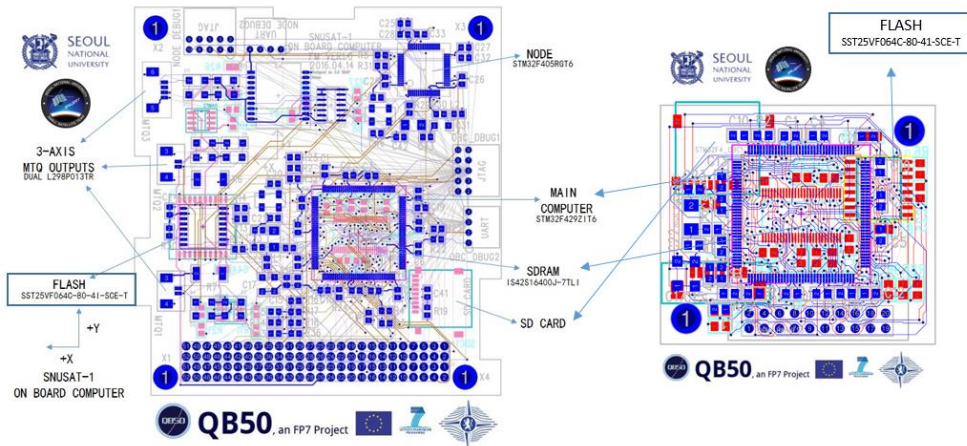
Figure 53 Comparative image shows processor, SDRAM, SD Card and flash all being re-implemented on the On-Board Computer design [Maskey, 2016]

6.2. Overview

This study provided a complete overview of designing an imaging payload for CubeSats in LEO. The focus has been to utilize COTS components to reduce development time and cost. Furthermore, the design principle is such that the camera should be modular and components from the camera such as processor, SDRAM, flash memory could also be used in other subsystem.

Chapter 1 introduced the requirements, provided a brief summary of CubeSat missions with imaging payload and underlying theory for building a camera.

Chapter 2 focused on the hardware, market research and how the components were selected. Tradeoff between component's market availability and performance had to be made. Often at times, ideal COTS components might not be available. If available, proper documentation might not be done. An overview of the hardware design, prototyping and also properties of the final hardware iteration for Flight Model was presented.

Chapter 3 touched on the software development of IFCAM. Software is based on layers of high level and low level library which help the user to interact with the hardware. This allows users to use high level language to give camera instructions. Algorithm of two modes; Mission Mode and Ground Testing Mode were presented and the key camera functions discussed.

Chapter 4 was on verifying the design. After integrating hardware and software, image was successfully obtained. However, the camera needed to be tested in outdoor and space environment conditions. Far field testing showed a need to reduce image brightness and also a need to place IR filter. Space environment tests included Random Vibration and Vacuum testing at SaTRec facilities in Daejon, Republic of Korea. No serious issues besides two loose bolts during vibration testing in the X and Y axis were seen.

Chapter 5 provided insight into how the system was further improved through the feedback received from Chapter 4. Relative target value for Auto Exposure setting was changed to -1.0. Optics from Edmund Optics with 650nm IR cut-off filter was used in order to remove IR noise on the image.

References

Aggarwal, P.K, "Dynamic (Vibration) Testing: Design-Certification of Aerospace System," NASA-Marshal Space Flight Center, 2011.

Botma, P.J.,"The Design and Development of an ADCS OBC for a CubeSat," Master Thesis, University of Stellenbosch, 2014.

Coderre, J., "The Radiation Environment of Space," MIT Lecture Note, 2006.

Dalsagar, H., et al., "Camera System for Pico Satellites," E4 2006 Project Report, Aalborg University, 2006.

Gimore, D.G., *Satellite Thermal Control Handbook*, The Aerospace Press, 2002.

Grobler, H., "Aspects Affecting the Design of a Low Earth Orbit Satellite On-Board Computer," Master Thesis, University of Stellenbosch, 2000.

Gulzar, K., "Camera design for pico and nano satellite applications," Master Thesis, Lulea University of Technology, 2009.

Joseph, G., *Building Earth Observation Cameras,* CRC Press, 2015.

Kimura, S., et al., "High-Performance Visual Monitoring System For IKAROS," Advances in Microelectronic Engineering, Vol. 1 No. 3, 2013, pp. 57-65.

Kimura, S., Miyasaka, A., "Qualification Tests of Micro-camera Modules for Space Applications," Transactions of the Japan Society for Aeronautical and Space Sciences, Aerospace Technology Japan, Vol. 9, 2011, pp. 15-20.

Kuuste, H., et al., "Imaging system for nanosatellite proximity operations," In: Proceedings of the Estonian Academy of Sciences, 2014, pp. 250-257.

Kuuste, H., "ESTCube-1 tether end mass imaging system design and assembly," Undergraduate Thesis, University of Tartu, 2012.

Maskey, A., "Feasibility Study of a Commercial Camera for Future CubeSat Missions," Undergraduate Thesis, Seoul National University, 2014.

Maskey, A., Park, J.H., Muruganandan V.A., Jeung I.S., "On-Board Computer Hardware Development using ARM Cortex M4 Processor(s)," The Korean Society for Aeronautical & Space Sciences 2016 Spring Conference, 2016.

Martinez, I., "Space Environment" Cuidad University Lecture Note, 2016.

Muruganandan, V.A., "Design of radiation tests for Photonic Mixer Device (PMD) based Imaging Sensor," Master Thesis, Julius-Maximilian's University of Wuerzburg, 2014.

Sarafin, T., Doukas P., Demchak L., Browning M., "Vibration Testing for Small Satellites", Instar Engineering and Consulting, Part 2, 2014.

Serway, R.A., Jewett, J.W., *Physics for scientists and engineers,* 6th edition, Brooks/Cole, Belmount, CA, 2004.

Terakura, M., et al, "Development and evaluation of a low-cost cots-based camera system for space applications," Advances in the Astronautical Sciences, Vol. 146, 2013, pp. 17-25.

Terakura, M., Kimura, S., "High-performance low-cost image processing unit for small satellite earth observation using cots devices," International Journal of Emerging Trends & Technology in Computer Science Vol. 1 No.2, 2013, pp.369-374.

Watanabe, S., et al., "Space Demonstration of Astronaut Extravehicular Activity (EVA) Support Robot," Mitsubishi Heavy Industries Technical Review Vol. 51 No.4, 2014, pp.33-42.

Wilson, D.R., "Vibration Testing For Small Satellites," Boing Aerospace Corporation, 1989.

초 록

본 논문에서는 큐브위성의 영상 탑재체에 대한 총괄 설계 연구에 대해 다룬다. 해당 영상탑재체는 궤도상에서의 기본적인 원격 탐지를 위해 설계되었으며, 서울대학교 최초의 큐브위성인 SNUSAT-1에 장착되어 영상 촬영 등의 추가 임무를 수행할 예정이다. 탑재체에 내장된 카메라는 2메가 픽셀 해상도의 MT9D111 이미지 센서를 사용하며, 측정한 영상정보를 처리하기 위해 180MHz로 구동되는 STM32F429ZI 프로세서를 사용하였다. 또한 촬영된 이미지는 기본적으로 내부 SRAM 버퍼에 저장되며, 외장 8MB SDRAM도 사용할 수 있도록 설계하였다. 본 시스템에서는 비휘발성 저장장치로 8MB 플래시 메모리와 4GB SD카드를 장착하였다.

초기 야외 실험에서는, 680nm 대역의 적외선 컷오프 필터가 필요한 것이 확인되었다. 광학계는 Edmund Optics 사의 마이크로 렌즈를 사용하는 것으로 수정하였으며, 이 때 지상샘플링거리는 650m, 지상관측폭은 570x400km로 남한 전역을 촬영할 수 있다. 진동 및 진공 환경 시험을 통해 시스템 설계 관련 특이사항이 없는 것으로 확인되었으며, 응용성을 가진 본 설계는 SNUSAT-1의 온-보드 컴퓨터 개발에 사용되었다.

주요어: 큐브위성, 영상탑재체, 원격 감지, 모듈 설계
학   번: 2014-25145

Appendices
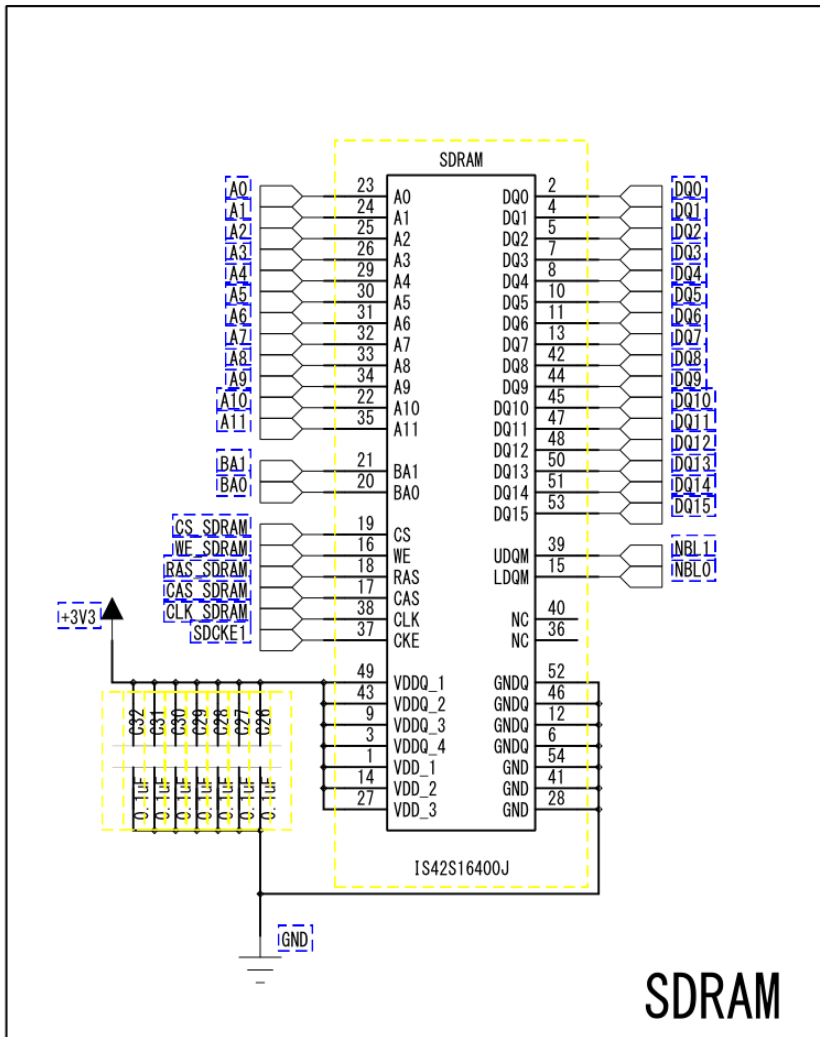
Figure 54 SDRAM schematics for IFCAM

72
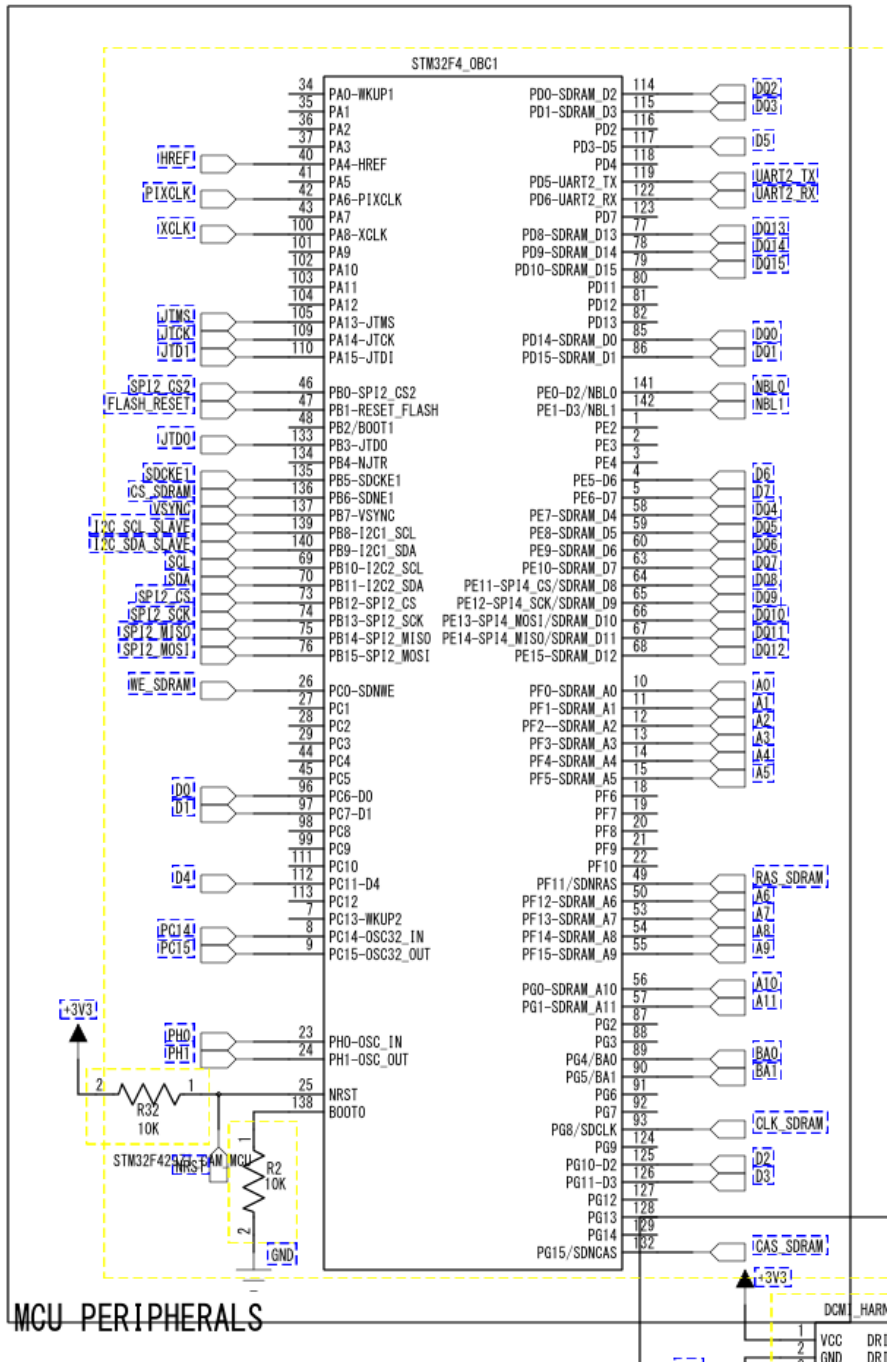
Figure 55 MCU Peripheral schematics for IFCAM

73
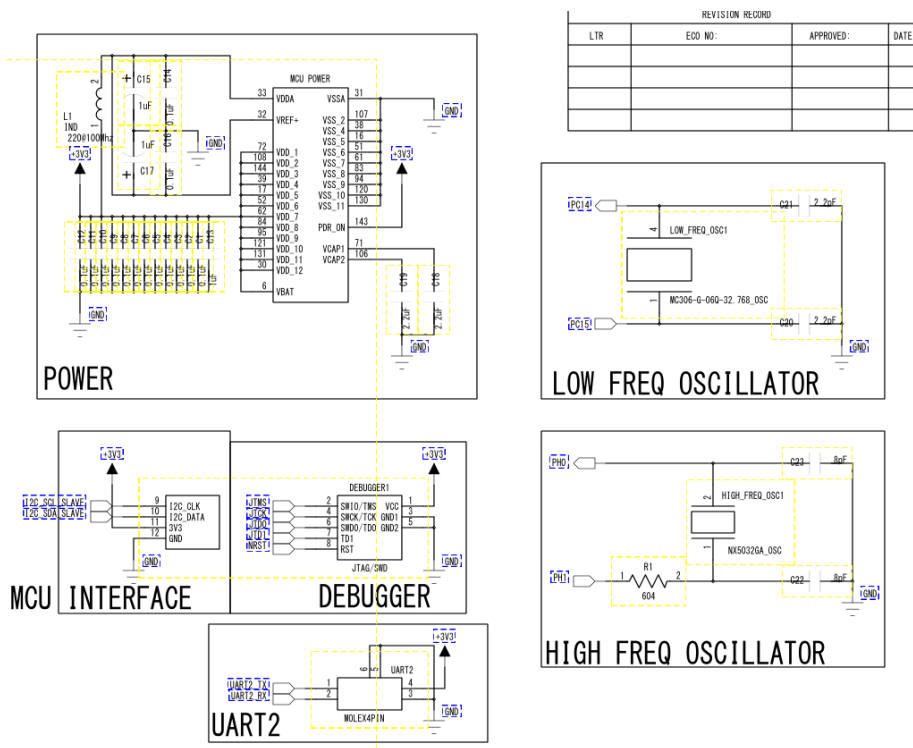
Figure 55 MCU power, oscillator, debugger and external interface schematics for IFCAM
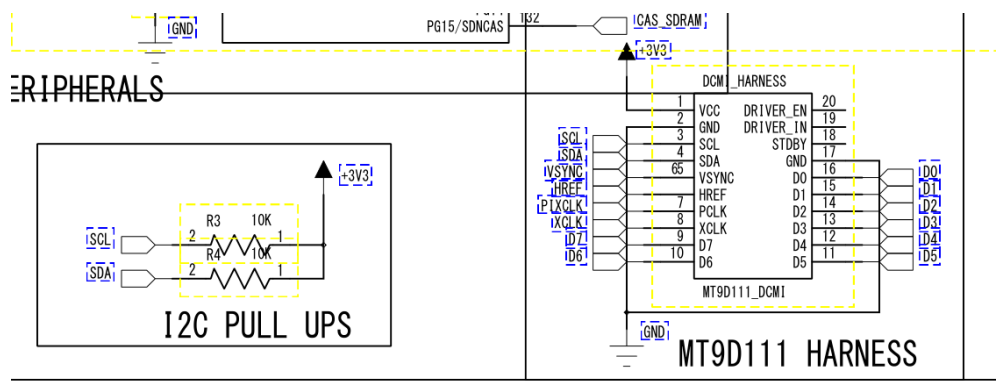

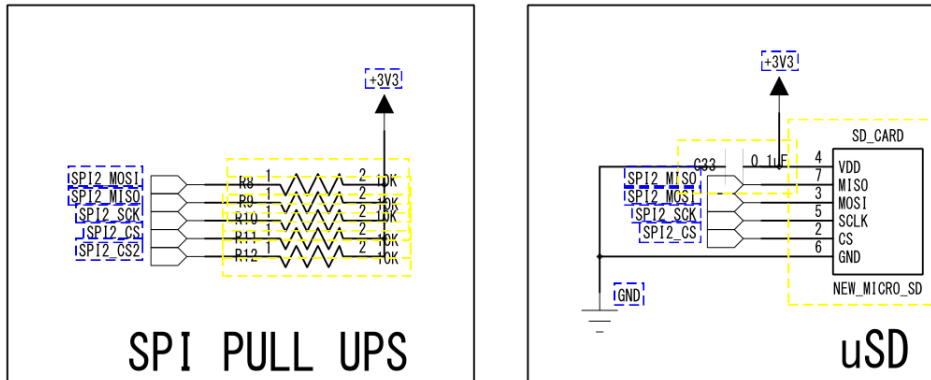**Figure 56** I2C pull ups, MT9D111 Harness schematics for IFCAM

74

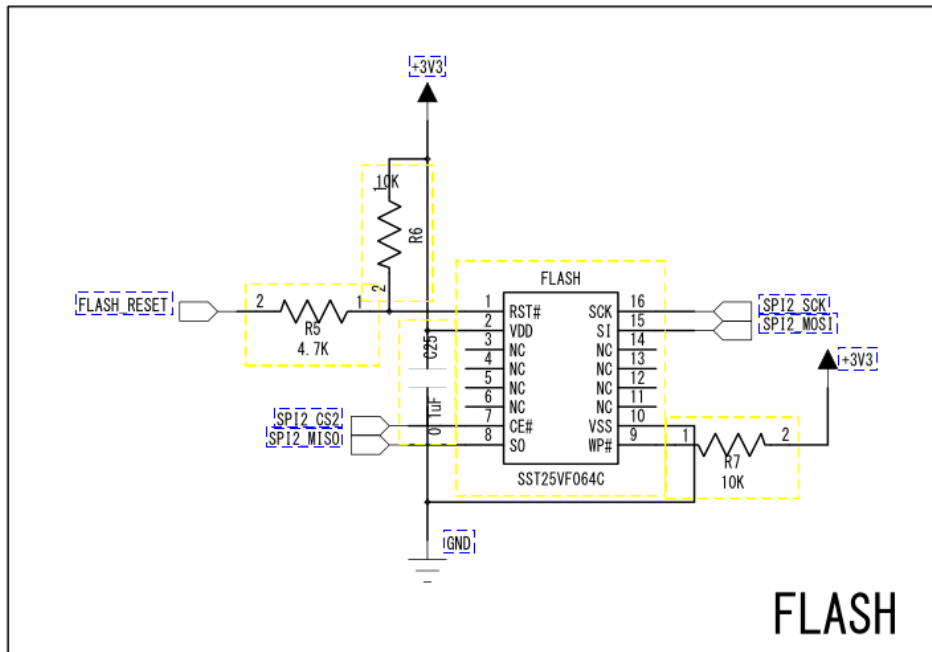**Figure 57** SPI pull ups and uSD schematics for IFCAM

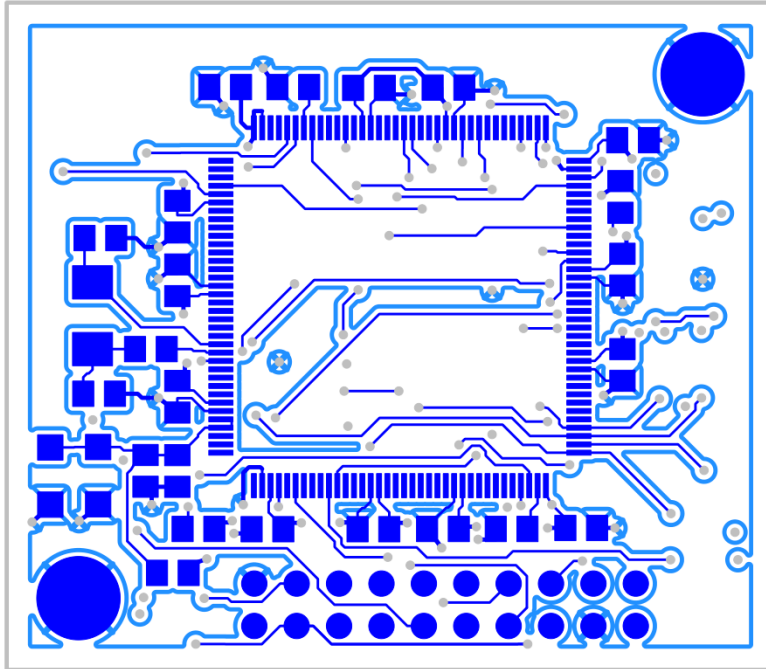**Figure 58** Flash schematics for IFCAM
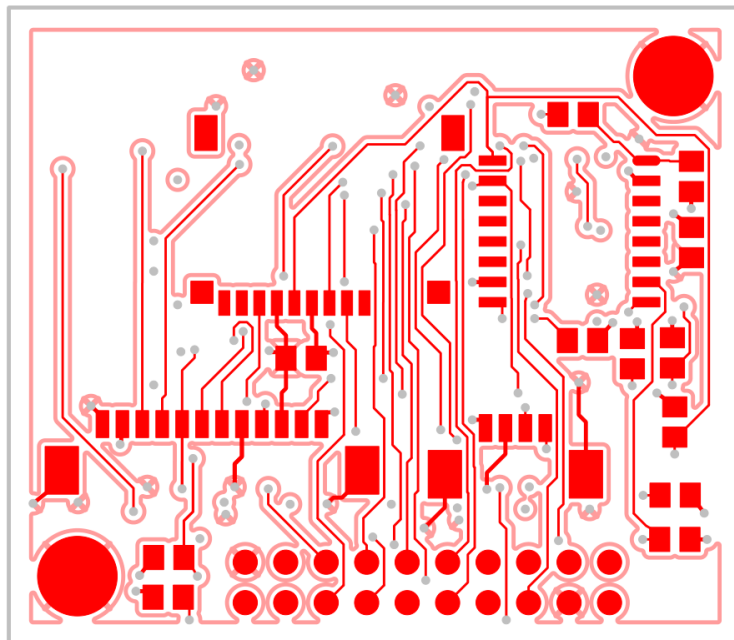
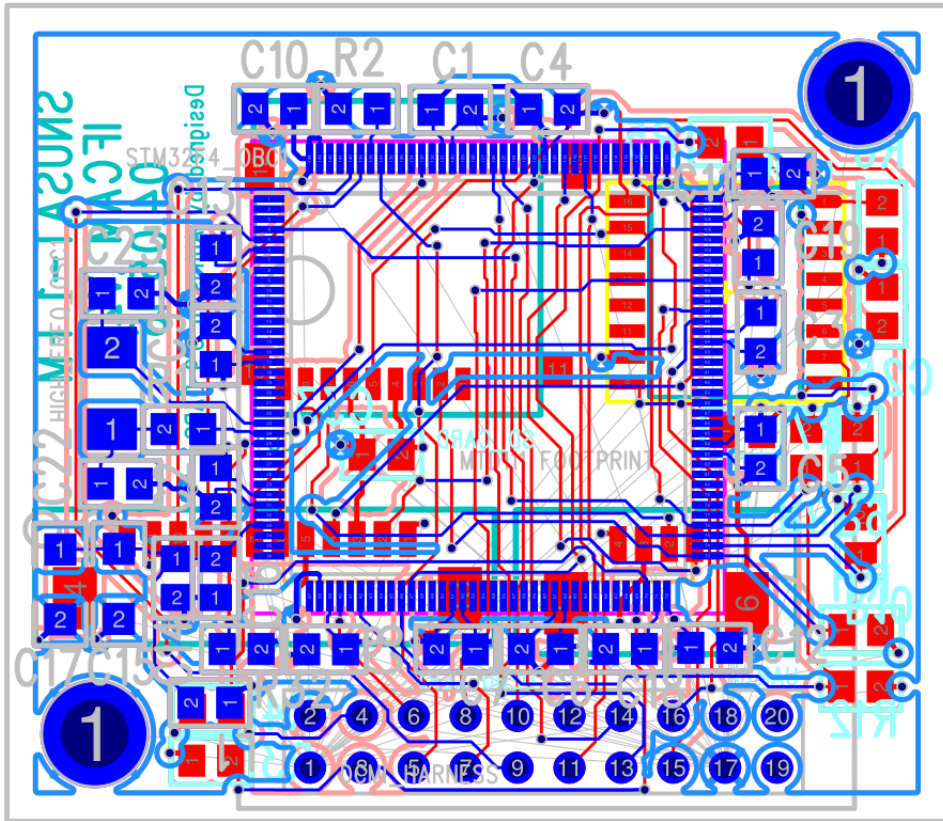**Figure 59** Top PCB layout for IFCAM

Figure 60 Bottom PCB layout for IFCAM

Figure 61 All layer layout for IFCAM

77